



This is a repository copy of *A Comparison of Contact Stiffness Measurements Obtained by the Digital Image Correlation and Ultrasound Techniques*.

White Rose Research Online URL for this paper:
<http://eprints.whiterose.ac.uk/94621/>

Version: Submitted Version

Article:

Mulvihill, D.M., Brunskill, H., Kartal, M.E. et al. (2 more authors) (2013) A Comparison of Contact Stiffness Measurements Obtained by the Digital Image Correlation and Ultrasound Techniques. *Experimental Mechanics*, 53 (7). pp. 1245-1263. ISSN 0014-4851

<https://doi.org/10.1007/s11340-013-9718-5>

Reuse

Unless indicated otherwise, fulltext items are protected by copyright with all rights reserved. The copyright exception in section 29 of the Copyright, Designs and Patents Act 1988 allows the making of a single copy solely for the purpose of non-commercial research or private study within the limits of fair dealing. The publisher or other rights-holder may allow further reproduction and re-use of this version - refer to the White Rose Research Online record for this item. Where records identify the publisher as the copyright holder, users can verify any specific terms of use on the publisher's website.

Takedown

If you consider content in White Rose Research Online to be in breach of UK law, please notify us by emailing eprints@whiterose.ac.uk including the URL of the record and the reason for the withdrawal request.



eprints@whiterose.ac.uk
<https://eprints.whiterose.ac.uk/>

A Comparison of Contact Stiffness Measurements Obtained by the Digital Image Correlation and Ultrasound Techniques

D.M. Mulvihill^{a,*}, H. Brunskill^b, M.E. Kartal^a, R.S. Dwyer-Joyce^b, and D. Nowell^a

^aDepartment of Engineering Science, University of Oxford, Parks Road, Oxford OX1 3PJ, UK

^bDepartment of Mechanical Engineering, University of Sheffield, Mappin Street, Sheffield S1 3JD, UK

Abstract:

The digital image correlation (DIC) and ultrasound techniques have both previously been employed to measure the contact stiffness of real engineering interfaces, but a comprehensive comparison of these techniques has not previously been carried out. Such a comparison is addressed in the present paper by a series of tests where both DIC and ultrasound are used to simultaneously measure contact stiffness in the same tests. The two techniques gave similar magnitudes for stiffness, with ultrasound being around three times stiffer at an average normal pressure of 70 MPa. Given that the techniques are vastly different in their measurement approach (DIC measures on the micron scale while ultrasound measures on the Ångstrom scale), this level of agreement is thought to be encouraging. The difference in results can partly be explained by consideration of physical differences between the techniques. Ultrasound measurement will give a local elastic ‘unloading stiffness’ whereas a load-deflection technique like DIC, will give a plastic ‘loading stiffness’. This difference is clearly brought out in the experiments carried out under increasing tangential load. Under normal loading, the increase in real contact area obscures the effect to some extent as both DIC and ultrasound stiffnesses increase with normal load. The results suggest that rough interfaces may be satisfactorily modelled as a variable stiffness spring whose stiffness increases with contact pressure as the smooth contact case is approached.

Keywords: Contact stiffness, Digital image correlation, ultrasound, titanium alloy

* Corresponding author. Tel.: +44 1865 2 73184; *E-mail address*: dm.mulvihill@yahoo.ie (D.M. Mulvihill).

1
2
3
4
5
6
7
8
9
10
11
12
13
14
15
16
17
18
19
20
21
22
23
24
25
26
27
28
29
30
31
32
33
34
35
36
37
38
39
40
41
42
43
44
45
46
47
48
49
50
51
52
53
54
55
56
57
58
59
60
61
62
63
64
65

Nomenclature

c	wave speed
f	coefficient of friction
f_u	ultrasound frequency
P	total normal force
p_m	mean normal pressure
Q	total tangential force
R	reflection coefficient
S_q	areal root mean square roughness (standard deviation of surface heights)
x, y, z	Cartesian coordinates, (z is normal to a surface)
Z	acoustic impedance
Z_1, Z_2	acoustic impedance in bodies 1 and 2
κ	contact stiffness per unit nominal area
κ_n	normal (longitudinal) contact stiffness per unit nominal area
κ_t	tangential (shear) contact stiffness per unit nominal area
κ_{DIC}	contact stiffness (per unit area) measured by digital image correlation
κ_{FE}	contact stiffness derived from a finite element model
$\kappa_{Interface}$	contact stiffness of an interface isolated from other contributions
ρ	density
ω	angular frequency

Abbreviations

DIC	digital image correlation
FE	finite element
FFT	fast Fourier transform
RMS	root mean square
UPR	ultrasound pulser-receiver

1. Introduction

Contact stiffness can be defined as the change in normal or tangential load at a contact for a unit change in relative normal or tangential displacement of the surfaces in contact. Defined in this way, contact stiffness depends on the position of the reference points for displacement. For a smooth contact model, the stiffness becomes infinite as these points approach the interface. However, real contacts are microscopically rough and this leads to a finite interfacial stiffness. The contact stiffness can either be defined as an instantaneous tangent stiffness at a particular load value or as a secant stiffness taken over range of load. Contact stiffness is a particularly important parameter in the analysis of jointed structures. The vibration response (resonant frequencies etc.) of single components can be predicted extremely accurately, but when frictional joints are present, current predictive models are often unsatisfactory due to a lack of understanding of joint parameters such as contact stiffness and friction [1]. Some of the friction issues have been addressed elsewhere (e.g.[2, 3]) and here we intend to focus solely on the stiffness aspects. These are particularly important in, for example, the aerospace industry where there are a number of frictional joints which have a direct bearing on vibration response (e.g. blade-disc dovetail joints, blade underplatform dampers, and blade-tip shrouds etc. in the aeroengine, as well as bolted or riveted joints in the aircraft structure). In order to further improve physical understanding of contact stiffness, techniques for its experimental measurement must be well developed and understood. Two methods which have been applied to real engineering interfaces are the digital image correlation [4-6] and ultrasound techniques [7-17].

Ultrasound is a vibration whose frequency is above the audible range. In a 1971 study, attempting to use ultrasound to measure the real area of contact at an interface, Kendall and Tabor [7] realised that the amount of ultrasound reflected from a rough interface was directly related to the stiffness of the interface. Since a given contact stiffness can be achieved with a single large area of contact, or with a smaller area divided into a number of contact regions which are spaced apart, they concluded that the technique could not hope to directly determine the real area of contact. However, the ability to measure contact stiffness was a promising development and Tattersall [18] went on to further define and generalise how this might be done. Essentially, these two early works proposed that the interface be considered as a region having the stiffness of a simple Hookean spring (see Figure 1).

1
2
3
4 When an incident ultrasound wave passes to a region of different material stiffness (or
5 density) through a perfect (smooth) interface, some of the wave is transmitted through, while
6 the remainder is reflected. The proportion of the incident wave which is reflected (called the
7 reflection coefficient) is directly related to the stiffness and density of each material.
8 Similarly, when an ultrasonic wave is projected through a rough interface, the contact
9 stiffness, as well as the stiffness and mass properties of the two materials, will determine the
10 reflection coefficient. Tattersall [18] used the 'spring model' to develop a simple formula
11 expressing the reflection coefficient R in terms of the acoustic impedance of the two materials
12 in contact Z_1 and Z_2 (defined as the product of density and wave speed) and the interface
13 stiffness per unit area κ .
14
15
16
17
18
19
20
21

$$22 \quad R = \frac{Z_1 - Z_2 + i\omega(Z_1 Z_2 / \kappa)}{Z_1 + Z_2 + i\omega(Z_1 Z_2 / \kappa)}. \quad (1)$$

26 where ω is the angular frequency of the ultrasound. Note that wave speed (accounted for in
27 the acoustic impedance term) is determined itself by the stiffness and density properties of a
28 material. If, as in the case of the present work, the material on both sides of the interface is
29 the same, then Equation (1) reduces to:
30
31

$$32 \quad R = \frac{1}{\sqrt{1 + \left(\frac{2\kappa}{\omega Z}\right)^2}}. \quad (2)$$

38 Solving explicitly for contact stiffness gives:
39
40

$$41 \quad \kappa = \frac{\omega Z}{2} \sqrt{\frac{1}{R^2} - 1}, \quad (3)$$

46 and substituting $\omega = 2\pi f_u$ and $Z = \rho c$ gives:
47
48

$$49 \quad \kappa = \rho c f_u \pi \sqrt{\frac{1}{R^2} - 1}, \quad (4)$$

53 where, f_u is the ultrasound frequency, ρ is the material density, and c is the wave speed in the
54 material. Equation (4) can be used for the calculation of both normal stiffness per unit area κ_n
55 and shear stiffness per unit area κ_t by simply using the appropriate transducer type and wave
56 speed c (i.e. longitudinal or shear). Therefore, from experiments in which the incident wave
57
58
59
60
61
62
63
64
65

1
2
3
4 and the reflected wave from a rough surface are recorded, the reflection coefficient R can be
5 found, and Equation (4) used to determine the contact stiffness.
6

7
8 The interface model described above is quasi-static and ignores any influence of mass.
9 Drinkwater *et al.* [12], used broadband transducers to examine frequency dependence in a
10 single test by calculating reflection coefficients and stiffness across the frequency range of
11 the transducer. They found that the reflection coefficient depended on frequency in the same
12 way as predicted by the ‘spring model’, but showed that contact stiffness was independent of
13 the frequency – thereby verifying the quasi-static ‘spring model’. There are, however, some
14 limitations on the frequency range which will give acceptable results. A succinct discussion
15 of this is given in Drinkwater *et al.* [12]. If the wavelength of the ultrasound is similar to the
16 size of the interface gaps, then complex scattering will occur where resonances are
17 established between gaps (Rose [19]). If the wavelength is considerably smaller than the gap
18 sizes, the results will not be affected by the gaps; however, the frequencies required to
19 achieve this are of the order of GHz for most commonly occurring machined finishes on
20 metals. At frequencies this high, the attenuation of the signal is too great to measure
21 meaningful results. If wavelengths significantly greater than the gap sizes are used, however,
22 then the reflection and transmission of ultrasound will be unaffected by the size, shape and
23 distribution of gaps, and attenuation of the signal will be low. Therefore measurements are
24 generally taken in the low frequency/long wavelength regime. Most work has been done on
25 metals and the frequency range of the transducers is usually 1–20 MHz [11-17].
26
27
28
29
30
31
32
33
34
35
36
37
38

39
40 The ultrasound method has more often been used for the calculation of normal contact
41 stiffness, but the approach is equally applicable to tangential stiffness as long as an
42 appropriate ultrasonic shear transducer is used and the wave speed in shear is used in
43 calculating acoustic impedances. The response of a rough contact to shear waves was
44 investigated successfully by Królikowski and Szczepek [11], Baltazar *et al.* [14], Dwyer-
45 Joyce and Gonzalez-Valadez [16], and Gonzalez-Valadez *et al.* [17]. One of the major
46 advantages of the ultrasound technique (which was referred to in the original paper by
47 Kendall and Tabor [7]) is that it can be applied to such a wide range of materials (i.e. metals
48 and non-metals, transparent materials and opaque materials).
49
50
51
52
53
54
55

56 The digital image correlation technique has only recently been used to measure contact
57 stiffness. Kartal *et al.* [4] appear to have been the first to use the technique, but further work
58 by Kartal *et al.* [5] and de Crevoisier *et al.* [6] has followed. The DIC technique involves
59
60
61
62
63
64
65

1
2
3
4 obtaining high resolution digital images giving side-on views of the interface (and the
5 surrounding area) while the applied load is varied. By comparing subsequent images to one
6 taken at the beginning of loading, displacements can be calculated on each side of the
7 interface and then subtracted to give local relative displacement. Applied load is easily
8 measured by a load cell; a plot of load versus relative displacement is then constructed and
9 the slope of the curve gives the contact stiffness. Each of these three papers used the DIC
10 technique for calculation of tangential contact stiffness during fretting tests (in gross sliding
11 with flat-and-rounded pads contacting a flat in Kartal *et al.* [4, 5], and in partial slip for a
12 single-bolt double lap joint in de Crevoisier *et al.* [6]).
13
14
15
16
17
18
19

20 The DIC and ultrasound techniques are radically different in their approach. Although
21 measurements of relative displacement can be taken local to the contact interface using DIC,
22 they are still somewhat remote from the contact compared to ultrasound, which derives its
23 measurements directly via wave reflection from the interface itself. In addition,
24 displacements on the micron scale are usually imparted in determining the load-deflection
25 curve for DIC, while those involved in an ultrasound excitation are of the order of
26 Ångstroms. Further, DIC measures from a single free surface orthogonal to the interface,
27 while ultrasound measurements are taken from an interior region of the interface.
28
29
30
31
32
33
34

35 Given the differences in the techniques, there is considerable interest in comparing
36 measurements taken using each. Despite this, there appears to be no available literature in
37 which contact stiffness measurements derived from load-deflection data (such as by DIC) are
38 compared to ultrasonically obtained stiffness values in the same test. It is possible only to
39 perform a very rudimentary comparison of the results from the two techniques by comparing
40 work by various researchers where the materials and contact configurations vary. For
41 example, the DIC results of Kartal *et al.* [4, 5] can be compared to the ultrasound results of
42 Gonzalez-Valadez *et al.* [17] and Baltazar *et al.* [14]. Kartal *et al.* [4, 5] were using Ti-6Al-
43 4V with flat-and-rounded pads in contact with a flat, Gonzalez-Valadez *et al.* [17] were using
44 steel-on-steel with a cylindrical punch-on-flat configuration, and Baltazar *et al.* [14] were
45 using aluminium-on-aluminium also with the cylindrical punch-on-flat arrangement.
46 However, it is possible to compare these results at the same average contact pressure of (70
47 MPa). At this pressure, Kartal *et al.* [4, 5] measured normalised stiffness values in the range
48 8–12 kN/mm³, Gonzalez-Valadez *et al.* [17] measured a range of 180–650 kN/mm³, and
49 Baltazar *et al.* [14] noted a range of 200–700 kN/mm³.
50
51
52
53
54
55
56
57
58
59
60
61
62
63
64
65

1
2
3
4 The figures quoted above suggest that ultrasound measurements may give higher stiffness
5 values. However, apart from the difference in material, surface roughness, and contact
6 configuration, there are some other differences: the results quoted from Kartal *et al.* [4, 5] are
7 averages from in excess of 5000 gross-slip fretting cycles at constant normal pressure, while
8 Gonzalez-Valadez *et al.* [17] and Baltazar *et al.* [14] took their results in a non-fretting
9 situation with zero bulk tangential load applied. Since ultrasonic shear waves apply an
10 Ångstrom scale tangential displacement to the interface, this means that the results in
11 Gonzalez-Valadez *et al.* [17] and Baltazar *et al.* [14] should be equivalent to the tangent
12 stiffness of the load-deflection curve at the very onset of bulk tangential load application;
13 whereas, the stiffness values reported in Kartal *et al.* [4, 5] were secant stiffness
14 measurements taken from a number of points on the load-deflection curve in a finite region
15 after the onset of tangential load application (which would be likely to give a lower stiffness).
16 In addition, wear debris may have reduced the contact stiffness in the experiments of Kartal
17 *et al.* [4, 5]. Hence, there are some reasons for the differences reported, but a comprehensive
18 study comparing the two techniques is required. Further, most of the ultrasound work has
19 been performed where normal load is either monotonically increased or cycled with no
20 applied tangential loading, and there appear to be no studies available which address the
21 effect of tangential loading on ultrasonically measured contact stiffness.
22
23
24
25
26
27
28
29
30
31
32
33
34

35 A key difference between the contact stiffness results derived from tangent values of load-
36 deflection results and those measured using ultrasound was suggested by Kim *et al.* [15].
37 These authors realised that an ultrasound wave actually imparts a small scale load-unload
38 cycle upon the bulk static load. Therefore, if the load-deflection curve is elastic both
39 methods should measure the same stiffness. However, if there is plasticity or some source of
40 irreversibility, the ultrasound can be expected to measure the local unloading stiffness while
41 the load-deflection technique will be measuring the tangent stiffness of the loading curve.
42 Although Kim *et al.* [15] demonstrated the difference by comparing the contact of two elastic
43 spheres (equivalent to the ultrasound unloading stiffness) and two elastic-plastic spheres
44 (equivalent to the load-deflection tangent stiffness), no direct experimental evidence
45 demonstrating the difference has so far been reported.
46
47
48
49
50
51
52
53
54

55 In the present work, the outstanding issues discussed above are addressed by a programme of
56 tests where DIC and ultrasound are used concurrently to measure contact stiffness in
57 unidirectional (i.e. non-fretting) 'first load-up' tests on Ti-6Al-4V flat-and-rounded contacts.
58 By assessing the level of agreement in trends and magnitudes between the techniques, the
59
60
61
62
63
64
65

1
2
3
4 experiments aim to learn more about what each technique is measuring. Both normal and
5 tangential contact stiffness is investigated under separate application of normal and tangential
6 loading; thereby allowing some other aspects of the physics of contact stiffness to be
7 investigated.
8
9

10 11 12 13 14 **2. Overview of the experimental setup**

15
16 In order to compare ultrasonically measured contact stiffness with contact stiffness measured
17 by DIC, a test was conceived whereby both measurements could be taken from the same
18 contact and during the same test. The setup is similar to that of Kartal *et al.* [4, 5] as the
19 same basic pad geometry and test machine were used. Figure 2 shows a schematic diagram
20 giving details of the configuration. As in [4, 5], the pad surfaces were flat, rectangular in
21 shape, with two parallel rounded edges and two 90 degree edges. These pads made contact
22 with a prismatic specimen with flat sides so that a plane surface is available for the DIC.
23 Digital images of a field of view (FOV) local to the contact interface are captured to allow
24 contact stiffness to be measured by DIC, while an ultrasonic transducer mounted to the back
25 face of the each of the pads allows simultaneous contact stiffness measurement of the same
26 interface by ultrasound. Also included in the design is the facility to control the tangential
27 load Q and the normal load P on each of the two contact interfaces.
28
29
30
31
32
33
34
35
36

37
38 In the tests carried out in [4, 5], the normal load P was transferred to each pad directly via its
39 back-face. However, in this case the loading was applied to an annular region of the pad
40 (Figure 2) by the front face of the pad-holders. This allowed a load free area at the back of
41 the pad for the ultrasound transducers. Figure 3 shows a photograph of a specimen in contact
42 with two pads. The specimen mounting thread, annular pad loading region, ultrasonic
43 transducer, and lead wires can be seen. Pads and specimens were designed so that two sizes
44 of contact area could be tested: 80 mm^2 and 50 mm^2 . For the 80 mm^2 area, the contact patch
45 was a rectangle of length 8 mm and depth 10mm while for the 50 mm^2 interface, geometric
46 similarity was maintained and the contact rectangle was 6.32 mm by 7.90 mm. The distance
47 between the two contacts was always 10mm.
48
49
50
51
52
53
54

55
56 The pads and specimens were manufactured from the aerospace titanium alloy Ti-6Al-4V.
57 The mechanical and chemical properties of the Ti-6Al-4V used here are given in Table 1.
58 Both pad and specimen surfaces were ground to a nominal area based root mean square
59
60
61
62
63
64
65

1
2
3
4 (RMS) roughness S_q of 2.3 μm . The test equipment used to provide the required constraints,
5 to apply and measure the loads (P and Q), and to capture the digital images is shown in
6 Figure 4. The details shown earlier in Figure 2 are housed inside a ‘work-holding block’
7 which allows the pad-holders to slide in the direction normal to the contact interface to
8 accommodate the normal loading which is applied by the hydraulic pistons shown (the value
9 is determined by a pressure gauge). Figure 4 also shows the hydraulic actuator and load cell
10 used to apply and measure tangential load, respectively. The load cell was calibrated for a
11 full-scale range of 0-15 kN with a resolution of 1N.
12
13
14
15
16
17
18
19
20

21 **3. Experimental procedures for ultrasound measurements**

22
23
24 Since the aim of the experiments is to measure both normal and tangential contact stiffness,
25 both longitudinal and shear ultrasonic transducers were used. These transducers were
26 commercial, broadband, piezo-ceramic transducers supplied by Tribosonics, UK and were
27 used as both transmitter and receiver (i.e. pulse-echo mode). The centre frequency for the
28 longitudinal and shear transducers was approximately 9.6 and 2.3 MHz, respectively (except
29 for the shear transducers used in tests 4, 5, 6, and 10 where a 5.2 MHz approx. shear
30 transducer was used – see Table 2 for an outline of the testing programme). The bandwidth
31 for the longitudinal and shear transducers (measured to a 6 dB reduction in amplitude) was
32 approximately 4–6 MHz and 2–3 MHz, respectively. Transducers for the 80 mm² contact
33 area pads were 4 mm × 4 mm in size and those for the 50 mm² contact were 3.16 mm × 3.16
34 mm; scaling the transducers in this way was carried out so that the signals would encounter
35 the same fraction of the contact width in each case. An electrical connection to the top and
36 bottom transducer faces is required to apply a voltage signal across the transducer which is
37 then converted to a mechanical vibration by the piezoelectric property of the transducer
38 material. The transducers were of the ‘wrap around electrode’ type so that both wires could
39 be soldered directly to the top face even though one of these connections makes electrical
40 contact with the bottom face only. The transducers were glued to the centre of the back face
41 of the pads (which had been smooth ground in preparation) using a cyanoacrylate based glue.
42 Two lead wires (Filotex 50 VMTX miniature PTFE coaxial cable) were then soldered to the
43 transducer which was then encased in epoxy to protect the connections and the transducer.
44
45
46
47
48
49
50
51
52
53
54
55
56
57
58
59
60
61
62
63
64
65

1
2
3
4 Since the setup incorporates two contacts, a shear transducer was always placed on one pad
5 and a longitudinal on the other. Only the right-hand contact was used for DIC, however, so
6 the appropriate type of ultrasonic transducer for the measurement being made (i.e.
7 longitudinal or shear) was used here, while the left-hand pad contained a transducer of the
8 other type. Two ultrasonic pulser-receivers (UPRs) were used to generate voltage pulses to
9 actuate the transducers. Equation (4) shows that the density and wave speeds for the material
10 are required in order to calculate contact stiffness. A density of 4420 kg/m^3 supplied by the
11 manufacturers, TIMET [20], was used. The speed of both longitudinal and shear waves in
12 the material were determined experimentally using the pads by sending a pulse to the surface
13 and back (a known distance) and recording the time taken. The measured longitudinal and
14 shear wave speeds in the material were 6148.28 m/s and 3092.8 m/s , respectively. Since the
15 spring model (Equation 4) relates reflection coefficient to stiffness, the main experimental
16 task is to determine the reflection coefficient when load is applied to the surface. The
17 reflection coefficient is simply the reflected wave divided by the incident wave (when the
18 amplitude information is expressed in the frequency domain). The incident wave data can be
19 obtained simply by recording the reflected wave from a metal-to-air interface, since the
20 acoustic impedance of air is very low in comparison to a metal such as Ti-6Al-4V. Hence, the
21 reflected wave in this case is equivalent to the incident wave. This ‘reference signal’ was
22 recorded before testing when the pads were not in contact with the specimen. Load was then
23 applied to the interface and the reflected signal was recorded for each load increment. The
24 incident and reflected signals (amplitude versus time) were then amplified by the UPR,
25 digitised by a digital oscilloscope, and passed to a computer for processing. A fast Fourier
26 transform (FFT) was subsequently implemented using LabView software to obtain the
27 frequency spectrum (amplitude versus frequency). The programme used the average of 50
28 successive pulses in obtaining the frequency spectrum. At each frequency, the amplitude of
29 the reflected wave was then divided by the amplitude of the incident wave to obtain reflection
30 coefficients which were then used to determine contact stiffness (Equation 4). The average
31 reflection coefficient across the bandwidth of the transducer (upper 6 dB) was then used to
32 calculate the contact stiffness for each load increment.
33
34
35
36
37
38
39
40
41
42
43
44
45
46
47
48
49
50
51
52
53
54
55
56
57
58
59
60
61
62
63
64
65

4. Experimental procedures for digital image correlation measurements

In order to measure contact stiffness using digital image correlation, images of the side face of the pad and specimen which include the contact interface are required during loading. For ease of analysis, the contact interface should be either vertical or horizontal in the images so that the x and y directions correspond to the normal and tangential directions. The interface should also be roughly in the centre of the images. To obtain the digital images during the tests a PixeLINK PL-B741U CMOS 1.3 mega-pixel monochrome digital camera [21] was used. This camera has a simple USB 2.0 interface and is based on the Cypress IBIS5 CMOS global shutter progressive scan sensor with a $2/3''$ optical format. This gave images of the field of view (FOV) with 1280×1024 pixels. In order to obtain high resolution, a Questar QM1 long distance microscope [22] with a variable zoom and a working distance of 150–355 mm was used as the lens to magnify a region local to the contact. The Questar (with the camera mounted) was fixed to a precision translation stage in order to allow focusing of the FOV (Figure 4). The optics were positioned as close as possible to the pad/specimen ‘side-surface’ to give maximum magnification. The resulting FOV (which was positioned at the centre of the right-hand interface) was approximately $1.3 \text{ mm} \times 1 \text{ mm}$ giving a pixel size of approximately $1.02 \text{ }\mu\text{m}$. Since the images contained no known macro-scale dimensions, calibration was carried out in two ways: by performing a known displacement of the specimen and dividing by the number of pixels moved, and by measuring the distance between two distinct surface micro-features using an Alicona optical profilometer and dividing by the equivalent number of pixels. Both techniques gave a very similar result.

The imaged surfaces of the pads and specimens were not specially prepared as the original grinding operation gave sufficient features for image correlation. Illumination of the FOV was provided by a fibre-optic illuminator which gave co-axial illumination. Images were recorded initially and also with each loading increment. The digital image correlation analysis of the images was then carried out using Imetrum Video Gauge software [23]. Crucially, this software allows the placing of targets on either side of the interface and can immediately output the relative displacement which occurs between a pair of targets. Figure 5 shows an image recorded from one of the tests showing all 20 targets used for analysis. The rectangular targets were 80×250 pixels in size while the four square targets shown were 80×80 pixels.

1
2
3
4 The algorithms used by the Imetrum Video Gauge software are proprietary, but in the
5 general, DIC software works by dividing an image into sub-regions. Relative displacements
6 are then determined by finding the best match for the reference image sub-region in the
7 deformed image. This is usually achieved by either maximising a cross-correlation type
8 function, or minimising a least-squares type function. The optimisation is usually performed
9 using some variation on the Newton-Raphson technique. However, an initial guess is
10 required for this technique; therefore, a two-step approach is usually used. Approximate
11 displacements with only integer level pixel accuracy are determined in the first step by
12 assuming zero displacement gradients and using a coarse searching method. In the second
13 step, the initial guess for the displacements is input as the starting point to the Newton-
14 Raphson method, however, since points may displace to sub-pixel locations, interpolation to
15 produce a continuous intensity function of grey levels in the deformed image must be
16 performed. Schemes such as bilinear interpolation or bicubic interpolation can be used here.
17 However, a higher-order interpolation scheme (e.g. bicubic spline or biquintic spline
18 interpolation) is recommended (Schreier *et al.* [24] and Knasss *et al.* [25]) since they provide
19 higher registration accuracy and better convergence than simple interpolation schemes. The
20 result should be accurate displacement and gradient predictions for the sub-region, and by
21 analysing many sub-regions, a full-field map of displacements and strains can be computed
22 by the method. For the present purposes a full field analysis is not required and, in the
23 Imetrum Video Gauge software, a single average displacement value is output and assigned
24 to the centre of each target. More detail on the use of the digital image correlation technique
25 is given by in two recent reviews by Pan *et al.* [26] and Hild and Roux [27].

26
27
28
29
30
31
32
33 The relative displacement measurement used for the majority of the analysis which follows
34 was derived as an average of the relative displacements associated with each of the five pairs
35 of targets positioned closest to the interface (i.e. targets 1&2, 13&14, 15&16, 17&18 and
36 19&20). Five further target pairs (i.e. targets 3&4, 5&6, 7&8, 9&10, and 11&12) were also
37 positioned on the images in order to study the relationship between contact stiffness and
38 distance from the interface. It is difficult to obtain data from measurement points with a
39 spacing less than about 100 μm – This is because the interface has a finite thickness, and
40 sufficiently sized regions are required for image correlation. Plots of load (at a single
41 contact) versus relative normal or tangential displacement were produced for each experiment
42 and curves were fitted to the data (using Matlab) so that the tangent stiffness values could be
43 obtained as the slope of the curves at various points during loading. A rational polynomial
44
45
46
47
48
49
50
51
52
53
54
55
56
57
58
59
60
61
62
63
64
65

1
2
3
4 function (5th degree/5th degree) was found to give a satisfactory fit to the data. Stiffness
5 values were subsequently normalised by the nominal contact area to give stiffness per unit
6 area (i.e. the same units as the ultrasound stiffness values given by the spring model in
7 Equation 4). The resolution of the software quoted by Imetrum is one thousandth of a pixel
8 size. Therefore, given that the pixel size is 1.02 μm with the present setup, the quality of the
9 results will be limited only by any noise introduced to the images themselves by small
10 vibrations/movements during testing.
11
12
13
14
15
16
17
18

19 **5. Experimental programme**

20
21
22 A total of ten experiments were carried out as shown in Table 2. In contrast to the work of
23 Kartal *et al.* [4, 5], measurements were only taken during the first monotonic application of
24 the tangential load. This is because the ultrasound result depends on a reference signal, and
25 any significant surface wear would invalidate the initial reference signal. Tests 1–6 had an 80
26 mm^2 contact area, while tests 7–10 had a contact area of 50 mm^2 . In tests 1, 2, 7 and 8, the
27 normal load was held constant to maintain a mean contact pressure p_m of 70 MPa while the
28 tangential load was incrementally increased up to the point of slip. This allowed the
29 tangential contact stiffness to be measured simultaneously at the right-hand contact by both
30 ultrasound and DIC while normal stiffness was recorded by ultrasound (only) at the left-hand
31 contact. This procedure permitted investigation into the effect of increasing tangential load
32 on normal and tangential contact stiffness. In tests 3, 4, 5, 6, 9, and 10, no tangential load
33 was applied and the normal load was increased, allowing comparison of measurements of
34 normal contact stiffness by both techniques at the right-hand contact (except for tests 5 and 6
35 where DIC was not used); tangential contact stiffness was measured by ultrasound only at the
36 left-hand contact. This allowed investigation of the effect of normal pressure on both contact
37 stiffness components. Loading was increased manually (by the hydraulic actuator of the test
38 machine in the case of tangential load and by a hydraulic pump in the case of normal
39 loading). At each load increment a digital image and a sequence of reflected ultrasound
40 pulses were recorded. The ultrasound pulses were recorded separately for each contact. Tests
41 were carried out on dry, unlubricated contacts with ambient pressure and temperature
42 conditions.
43
44
45
46
47
48
49
50
51
52
53
54
55
56
57
58
59
60
61
62
63
64
65

6. Results and discussion

Figure 6 shows an example of the type of displacement profile observed in the digital images along the normal to the centre of the contact patch when tangential load was applied. Some deformation occurs in the pad and specimen, but the large discontinuity in displacement at the interface is due to the compliance caused by the rough surface interaction. It can be seen that relative displacement between points closest to the interface is dominated by this interface contribution.

Figure 6 shows tangential displacement of the pad and specimen for a particular value of tangential load (corresponding to $Q/fP = 0.48$) in Test 1. Figure 7, however, shows the full variation of relative tangential displacement (for the measurement points closest to the interface) with applied tangential load for each of the four tests where tangential load was increased monotonically towards slip (Tests: 1, 2, 7, & 8). The average coefficient of static friction in these four tests was 0.24 – less than the values determined for Ti-6Al-4V in Kartal *et al.* [4] which reached a steady average of about 0.6 in gross-slip fretting tests. This is because a ‘run-in’ period is required before the contact reaches an approximate steady state, but in the present tests only the initial loading is considered so that the friction remains low. The data in Figure 7 show a distinct trend even though the relative displacements are very small (increasing to a maximum of between 2–3 microns near to the point of slip). It can be seen also that the force-displacement curves here are distinctly non-linear and suggest plastic deformation. Since all the results in this section correspond to initial loading of the contacts, this plastic flow is to be expected. Also shown (in red) are the rational curve fits which were used to determine tangent stiffness at each load increment.

The resulting variation in tangential contact stiffness (obtained by DIC) with tangential load for these four tests is shown in Figure 8 together with the corresponding ultrasound stiffness values derived simultaneously from the same contact. It can be seen that as tangential loading on the contact is increased, the contact stiffness as measured by DIC decreases. The ‘ultrasound stiffness’, on the other hand, does not decrease correspondingly, and instead either remains almost constant or increases somewhat.

A possible reason for this difference was first proposed by Kim *et al.* [15] as discussed earlier. They pointed out that since rough contacts quickly become elasto-plastic as loading is increased, and because ultrasound applies a local loading-unloading cycle centred on the

1
2
3
4 static stress, the ‘ultrasonic interfacial stiffness’ is actually measuring the local unloading
5 stiffness. This will be an elastic stiffness since the stress state is taken back inside the yield
6 locus by the small scale perturbation (of the order of Ångstroms) supplied by the ultrasound.
7 This local unloading stiffness does not ‘feel’ the plastic softening of the asperities, and
8 therefore, even though the tangent stiffness of the loading curve decreases due to plastic
9 yielding of asperities, the local unloading stiffness would not be expected to change as the
10 tangential load is increased. This is explained schematically in Figure 9.

11
12
13
14
15
16 Therefore, the closest agreement between ultrasound and DIC can be expected at the onset of
17 tangential loading ($Q = 0$) where tangent stiffness and unloading stiffness are expected to be
18 approximately equal. The effect discussed here, though proposed by Kim *et al.* [15] in a
19 discussion of normal contact stiffness, had not previously been observed experimentally.
20 Previous investigations have tended to focus, not on the variation of tangential contact
21 stiffness with tangential load, but instead on the variation with normal load where the effect
22 could be expected to be masked by the significant increase in the real area of contact which
23 occurs during normal loading. This would tend to cause both the ‘ultrasonic stiffness’ and
24 the tangent stiffness of the loading curve to increase with load. In any case, to confirm the
25 effect, an independent technique to measure the tangent stiffness of the loading curve
26 concurrently with the ultrasound measurements is required. The use of DIC in conjunction
27 with ultrasound in the present work has permitted this comparison to be made. A moderate
28 increase in ultrasonically measured shear stiffness is seen to occur in Figure 9a, b, and d.
29 This may be due to a slight increase in contact area with tangential load owing to junction
30 growth as first observed by McFarlane and Tabor [28]. This increase in contact area is small
31 in comparison to that which would be expected in normal loading. The evolution of the
32 normal contact stiffness with tangential load measured by ultrasound in Tests 1, 2, 7, and 8 is
33 given in Figure 10. This stiffness is relatively unaffected by tangential load and good
34 repeatability can be seen across the four independent tests.

35
36
37
38
39
40
41
42
43
44
45
46
47
48
49
50 Figure 11 shows normal force versus relative normal displacement for the four tests where
51 both DIC and ultrasound were used to measure normal stiffness (i.e. Tests: 3, 4, 9, and 10).
52 Again, despite the small displacements involved, a definite trend is apparent in the raw data.
53 The rational curve fits from which tangent stiffness values were obtained are also shown.
54 Figure 11a shows that good agreement is observed when the ‘Imterum DIC results’ are
55 compared to those from a different software package (DaVis StainMaster by LaVision [29]).
56
57
58
59
60
61
62
63
64
65

1
2
3
4 These two packages use different algorithms for the calculations of displacements and their
5 agreement in Figure 11a increases confidence in the results.
6
7

8 Figure 12 compares normal contact stiffness derived from DIC analysis (slopes of the loading
9 curves) with that derived from ultrasound for tests 4 (contact area: 80 mm²) and 9 (contact
10 area: 50 mm²). As expected, both DIC and ultrasound stiffness increase in this case owing to
11 the increase in real area of contact with normal loading. The DIC stiffness is again greater
12 than the ultrasound stiffness but this may be due to the fact that the ultrasound technique does
13 not ‘feel’ the plastic softening of the asperities as it measures local unloading stiffness rather
14 than tangent stiffness as discussed above.
15
16
17
18
19

20
21 In Figure 13, ultrasonically measured tangential contact stiffness is plotted against normal
22 contact pressure for tests 3, 4, 6, and 9. Again, as expected, the stiffness values increase with
23 normal load and reasonable repeatability can be observed between the four tests. The
24 stiffness values in Figure 12 and Figure 13 appear to show fairly linear variations with
25 contact pressure unlike, for example, the results from Gonzalez-Valadez *et al.* [17] where the
26 stiffness varies approximately as the square root of contact pressure. This may be because
27 the material being tested here has a high yield strength (1000 MPa) and may not display any
28 softening behaviour until pressures greater than 200 MPa are reached. This is in agreement
29 with a recent elastic model of tangential contact stiffness ([5]), which is based on the
30 application of Mindlin’s solution [30] for tangential loading of Hertz contacts to the statistical
31 rough surface model of Greenwood and Williamson [31] using an exponential distribution of
32 asperity heights.
33
34
35
36
37
38
39
40

41
42 For the ultrasound measurements in both Figure 10 and Figure 13 (and for the DIC results in
43 Figure 8), there is no discernible difference between the stiffness per unit area results from
44 the 80 and 50 mm² contact areas: this suggests that the contact stiffness [load/distance] may
45 be proportional to nominal contact area – as was the case for the fretting situation in Kartal *et*
46 *al.* [5]. In Figure 14, contact stiffness measured by DIC is compared to that given by an
47 elastic ‘smooth contact’ finite element (FE) model of the pad-specimen experiment. Details
48 of this model have already been outlined in Kartal *et al.* [4] and the results shown in Figure
49 14 are from the FE model in [4] with 80 mm² contact area (without any additional layer to
50 represent the interface compliance). It should be noted that the ‘stiffness’ derived from the
51 FE model is that which is due *only* to displacement of the ‘bulk’ material situated between
52 measurement points which are deliberately spaced apart by the same amount as those in the
53
54
55
56
57
58
59
60
61
62
63
64
65

1
2
3
4 experiments. This is done so that the ‘bulk’ contribution to the experimentally measured
5 contact stiffness (found from the FE model) can be compared to the experimental result and
6 to the ‘true interface contact stiffness’. In Figure 14a and Figure 14b, tangential and normal
7 contact stiffness are plotted against distance between measurement points, respectively.
8
9

10
11 The DIC stiffness plots shown in Figure 14a are the initial tangential contact stiffness values
12 of the pre-sliding regime (i.e. slope of the loading curve at $Q = 0$) where tangent stiffness is
13 expected to be closest to the elastic ‘unloading stiffness’ (see Figure 9). The comparison of
14 the FE model to experimental results undertaken in Kartal *et al.* [4] was to tangential contact
15 stiffness results obtained during gross-slip fretting wear (normal pressure: 70 MPa) where the
16 experimental result was significantly less stiff than the elastic smooth contact FE prediction.
17 Here also, the DIC stiffness values are considerably less than the FE result for the 70 MPa
18 contact pressure, though they are greater (by about four times) than the corresponding DIC
19 stiffness values quoted in Kartal *et al.* [4] – the reason for this is discussed later. An ‘isolated
20 interface stiffness’ can be defined by considering the experimental interface stiffness (the
21 DIC stiffness κ_{DIC}) as the series sum of the ‘bulk stiffness’ (given by the FE result κ_{FE}) and
22 the true interface stiffness $\kappa_{\text{Interface}}$ (called the ‘isolated interface stiffness’ here):
23
24
25
26
27
28
29
30
31

$$\frac{1}{\kappa_{\text{DIC}}} = \frac{1}{\kappa_{\text{FE}}} + \frac{1}{\kappa_{\text{Interface}}}. \quad (5)$$

32
33 The ‘isolated interface stiffness’ is also shown in Figure 14 for the DIC result at 70 MPa
34 normal contact pressure, and this is again similar to the raw DIC result. It can therefore be
35 assumed that at a normal pressure of 70 MPa, the interface compliance is dominant and that
36 proportionality of stiffness [force/distance] with nominal contact area will hold in the same
37 way as for the fretting case in Kartal *et al.* [5]. However, Figure 14a also shows a DIC result
38 for a normal contact pressure of 200 MPa where the tangential contact stiffness is
39 considerably closer to the predicted FE result.
40
41
42
43
44
45
46
47
48

49 In the case of normal stiffness (Figure 14b) the experimental result at $p_m = 70$ MPa is
50 considerably less than the FE smooth contact stiffness, though again, as the normal pressure
51 is increased from 70 to 200 MPa, the experimental stiffness approaches the FE smooth
52 contact elastic result. As with tangential contact stiffness, both DIC and FE stiffness values
53 increase as the interface is approached by the measurement points – though the DIC stiffness
54 increases by much less than the FE as it becomes dominated by the interface compliance as
55 the interface is approached (this is also clear from the displacement profile which was shown
56
57
58
59
60
61
62
63
64
65

1
2
3
4 in Figure 6). In contrast, the smooth contact model assumed in the FE means that the
5 stiffness will tend to infinity as the reference points approach the interface.
6
7

8 Figures 12, 13 and 14 all show that both normal and tangential contact stiffness may be
9 considered as variable stiffness springs whose stiffness depends on the contact pressure.
10 Figure 14 helps to shed light on an important discrepancy between different results quoted in
11 the literature. Some authors (e.g. Johnson [32], and O'Connor and Johnson [33]) observed
12 that the remote load-displacement response of real contacts agreed well with a smooth
13 contact elastic analysis. Other authors, however, (e.g. Berthoud and Baumberger [34], and
14 Shi and Polycarpou [35]) have observed that the rough interface reduced the stiffness to well
15 below that of the elastic smooth contact predictions.
16
17
18
19
20
21

22 It is suggested here that it is the degree to which the contact area approximates the smooth
23 contact case that determines whether the contact stiffness will agree with elastic predictions
24 or be dominated by the rough interface. Essentially, as the real area of contact approaches the
25 apparent area of contact, a response similar to the smooth contact prediction would be
26 expected. Whether or not a contact approximates the smooth case probably depends on
27 factors such as contact pressure, material hardness and surface roughness. The suggestion
28 here is that at low normal pressures; high hardness; and high roughness, contact stiffness will
29 be controlled by the multi-asperity contacts of the rough interface, but at high normal
30 pressures; low hardness; and low surface roughness, these contacts will merge until the
31 contact becomes closer to the smooth contact case. When a contact is dominated by a multi-
32 contact interface, both micro-slip on the scale of the asperities (Campaña *et al.* [36]) and
33 extra compliance introduced by voids (Sevostianov and Kachanov [37]) tend to reduce the
34 contact stiffness to well below the smooth contact prediction (which is based purely on bulk
35 deformation). The hypothesis just outlined is consistent with Figure 14 where it can be seen
36 that at the lower normal pressure (70 MPa), the contact stiffness is lower and more dominated
37 by the rough interface, whereas at the higher pressure (200 MPa), the contact stiffness
38 appears to approach closer to the smooth contact FE result.
39
40
41
42
43
44
45
46
47
48
49
50
51

52 This analysis would also help explain the discrepancy arising from test results in the
53 literature. If we examine the results in the literature in more detail, the discrepancy can more
54 easily be understood. Of those authors who found agreement with the smooth contact
55 prediction, Johnson [32] was using smooth ball bearing type surfaces while O'Connor and
56 Johnson [33] used a very high mean contact pressure (472 MPa). Both these authors used the
57
58
59
60
61
62
63
64
65

1
2
3
4 sphere-on-flat arrangement. On the other hand, the authors who found that the interface
5 roughness dominated the measured contact stiffness were using very low contact pressures
6 (Berthoud and Baumberger [34] used mean pressures up to 0.04 MPa for their flat-on-flat
7 tests, and Shi and Polycarpou [35] used contact pressures up to 0.055 MPa for their sphere-
8 on-flat experiments). The authors of references [32-34] measured the response to tangential
9 loading while [35] measured the response to normal loading, and these observations, together
10 with the results in Figure 14, suggest that the conclusions being made here apply equally to
11 both normal and tangential contact stiffness. In summary, the effect which the rough surface
12 interface has upon the contact stiffness probably depends mainly upon contact pressure,
13 surface roughness and surface hardness.
14
15
16
17
18
19
20
21

22 Finally, some discussion of the comparison of stiffness magnitudes is warranted. First, it is
23 useful to compare DIC results obtained here at $p_m = 70$ MPa with available results on the
24 same material (Ti-6Al-4V) taken at the same normal contact pressure using similar optical
25 techniques in the literature. These are only available for tangential contact stiffness in gross-
26 slip fretting tests. Kartal *et al.* [4, 5] (using DIC), obtained values between 8–12 kN/mm³
27 closest to the interface using contact areas of 80 and 20 mm², and Proprentner [38] (by
28 tracking two laser points on either side of the interface) obtained values of 12–20 kN/mm³ on
29 a much smaller rig setup with a 1 mm² contact area. In the present work, values of 35–45
30 kN/mm³ were obtained (see Table 3). There are some important differences which explain
31 these higher values: first, the values quoted from the literature are from fretting wear tests
32 where wear debris will serve to reduce interface stiffness, and also, the authors in [4, 5, 38]
33 measured the initial secant stiffness at the beginning of micro-slip rather than the initial
34 tangent stiffness at the beginning of micro-slip. Another key difference is that the stiffness
35 results quoted in Table 3 are the initial tangent stiffness values at the very onset of the micro-
36 slip regime during initial loading of the contacts, whereas, those by Kartal *at al.* [4, 5] and
37 Proprentner [38] are the initial ‘unloading stiffness’ at the point of motion reversal during
38 fretting. This ‘unloading stiffness’ is generally expected to be elastic; though, wear debris is
39 a complicating factor.
40
41
42
43
44
45
46
47
48
49
50
51
52

53 Turning to the comparison of DIC and ultrasound stiffness magnitudes in the present work,
54 both can be graphically compared for tangential contact stiffness in Figure 8 and for normal
55 stiffness in Figure 12, and numerical values of measurements by the two methods are also
56 given for tangential and normal contact stiffness respectively in Tables 3 and 4 for $p_m = 70$
57 MPa, and $Q = 0$ (i.e. at the onset of tangential loading in the case of tangential stiffness).
58
59
60
61
62
63
64
65

1
2
3
4 Figure 8 and Table 3 both show that the DIC tangential contact stiffness is reasonably
5 repeatable in the four tests where it was measured. There is some degree of variability in the
6 ultrasound measurements of tangential contact stiffness and this may possibly be explained
7 by noting that ultrasound is very much a local measurement derived from a sub-region at the
8 centre of the interface (which will be similar in size and shape to the emitting transducer) and
9 will depend intimately on the contact which occurs in this region. Therefore, it can be
10 sensitive to specimen misalignment, and small changes in local roughness and waviness etc.
11 Since the DIC measurement is taken from points located some 50 microns or so from the
12 interface, it is less likely to vary since it depends more on the behaviour of the whole contact
13 region. On average (based on all data in Tables 3 and 4), the ultrasound is approximately 2.7
14 times stiffer than the DIC result for tangential stiffness and 3.5 times stiffer for normal
15 contact stiffness. However, given that the two techniques are widely different in their method
16 of measurement, the fact that the agreement in magnitude is this close is noteworthy.
17 Particular good agreement between DIC and ultrasound can be seen graphically for normal
18 stiffness in Figure 12. An analysis of available results in the literature was outlined in the
19 introduction where tangential contact stiffness data from separate ultrasound and DIC studies
20 were compared. Although those tests did not have the same materials; contact geometry;
21 surface topography; or testing regime, their finding that the ultrasound results were stiffer is
22 consistent with the conclusions being made here.
23
24
25
26
27
28
29
30
31
32
33
34
35
36

37 In attempting to understand why ultrasound gives a stiffer result, the following points should
38 be noted. As we have seen, ultrasound gives the local unloading stiffness, whereas DIC gives
39 the tangent stiffness. This argument can be used to explain the stiffer result for normal
40 stiffness; however, for tangential stiffness, as long as both stiffness values are determined at
41 the very onset of micro-slip ($Q = 0$), the effect should not be very important. In addition, the
42 DIC result is derived from points located some 50 microns or so into the bulk, whereas the
43 ultrasound result is derived directly from the interface itself where stiffness is expected to be
44 higher (Figure 14 illustrates the predicted rise in stiffness as the interface is approached) –
45 this argument applies to both normal and tangential stiffness. Also, in the case of tangential
46 loading, it is difficult to obtain an accurate stiffness by DIC at $Q = 0$ since the relative
47 displacement data can be difficult to interpret until Q is increased sufficiently (see Figure
48 6.14c).
49
50
51
52
53
54
55
56
57
58
59
60
61
62
63
64
65

7. Conclusions

In this work a comparison of concurrent DIC and ultrasound measurements was undertaken in a series of unidirectional ‘first load-up tests’ where either the normal or tangential load was incrementally increased. Despite the small displacements involved ($< 2\text{--}3\ \mu\text{m}$ up to slip in the case of tangential loading), the DIC technique was seen to produce distinct load versus relative displacement curves for both normal and tangential loading cases. The load-displacement curves were non-linear indicating plastic flow: as would be expected from initial loading of a rough contact. For the first time, a fundamental difference (proposed by [15]) between the tangent stiffness taken from the loading curve and the ‘ultrasonic stiffness’ was observed: ultrasound always measures the local unloading stiffness which is elastic and unaffected by the plastic softening of asperities tending to reduce the tangent stiffness. This effect was observed experimentally in the present work in the tangential loading case where DIC stiffness was seen to reduce towards zero as loading proceeded; whereas, the ultrasound saw no reduction in tangential contact stiffness. For normal contact stiffness, both DIC and ultrasound values increased with normal load due to the increase in real area of contact which masks this effect (though normal stiffness measured by DIC was less stiff than ultrasound at equivalent normal loads – probably owing to plastic softening lowering the DIC stiffness but not the ultrasound stiffness). In agreement with the work of previous researchers, tangential and normal contact stiffness were both found to increase with normal loading.

When compared to the DIC results derived by [4] during gross-slip fretting tests, the tangential contact stiffness values obtained here by DIC in the unidirectional tests were about four times stiffer – this may be due, among other things, to the tendency of wear debris in the fretting tests to reduce contact stiffness. The DIC results for contact stiffness arising from these unidirectional tests were also compared to stiffness values derived from a smooth contact FE model. For the lower contact pressure (70 MPa), the contact stiffness was dominated by the compliance of the rough interface. However, when the contact pressure was increased to 200 MPa, the contact stiffness approached closer to the smooth contact elastic FE result. This suggests that at low pressures the multi-asperity contacts dominate the contact stiffness, but as the pressure is increased, these contacts merge to form a contact which begins to more closely approximate the smooth contact case. Therefore, at lower normal contact pressures, the result that contact stiffness is proportional to nominal contact area can be true even for the non-fretting case; in fact, the results show that no discernible difference in ultrasound and DIC contact stiffness (per unit area) between the 80 and 50 mm²

1
2
3
4 contacts can be observed at 70 MPa. It was hypothesised (based on results here and in the
5 literature) that the degree to which contact stiffness depends upon bulk deformation (when
6 measured remotely) depends on how well the contact approximates the smooth contact
7 equivalent. Following from this analysis, it seems reasonable to suggest that the extent to
8 which the contact stiffness depends upon the interface will depend on three main factors:
9 contact pressure, surface roughness, and surface hardness.
10
11
12
13

14
15 Turing finally to comparison of magnitudes, given the vast difference between the two
16 methods, the fact that corresponding stiffness values are of the same order of magnitude is
17 firstly of interest. Ultrasound was always stiffer than DIC: on average, for normal stiffness,
18 the ultrasound result at $p_m = 70$ MPa was about 3.5 times stiffer than DIC, and for tangential
19 stiffness, the ultrasound result at $p_m = 70$ MPa was 2.7 times stiffer. This disagreement is
20 sufficiently small so that a question cannot be raised about the validity of either method
21 especially given that ultrasound measures local unloading stiffness whereas DIC measures
22 tangent stiffness. However, it does seem that there is quite a degree of variability in the
23 ultrasound measurements which are probably more sensitive to local contact and roughness
24 conditions than DIC. DIC may be more robust in certain circumstances since its
25 measurement depends more on the entire contact (as the measurement points are somewhat
26 removed from the surface). There are disadvantages to the DIC technique also, such as the
27 fact that a reliable tangential contact stiffness measurement at the very onset of micro-slip is
28 difficult to determine due to the small displacements and the 'slack' involved before the load
29 is sufficiently increased. Choosing which technique to use in a given case will depend on
30 which technique can be physically accommodated. Also if tangent stiffness is required, DIC
31 is the obvious choice, whereas ultrasound is suited to measuring the elastic local unloading
32 stiffness. In addition, DIC is more suited to measuring contact stiffness in fretting tests as the
33 ultrasound reference signal is invalidated by surface wear in fretting.
34
35
36
37
38
39
40
41
42
43
44
45
46
47

48 To improve comparison between ultrasound and digital image correlation measurements of
49 contact stiffness, more focus should be given to making the comparison during unloading
50 rather than loading since the quantity being measured by each technique should be more
51 similar. A comprehensive study on how factors such as contact pressure, surface topography,
52 surface hardness, and surface chemistry affect the extent to which remotely measured contact
53 stiffness departs from theoretical smooth contact predictions would also be useful.
54
55
56
57
58
59
60
61
62
63
64
65

Acknowledgments

The authors would like to acknowledge the financial support of the Engineering and Physical Sciences Research Council (EPSRC) under grant reference EP/E058337/1: "A Predictive Approach to Modelling Frictional Joint Performance (PAMFJP)". Mr Richard Duffin and Mr Wolfgang Mix and also thanked for their work on machining the various test components. Thanks are due also to the British Society for Strain Measurement (BSSM) and Imetrum Ltd for providing the digital image correlation software as part of the 2011 Young Stress Analyst Competition first prize which was awarded to the first author.

References

- [1] Segalman, D. J., Bergman, L. A., and Ewins, D. J., 2007, "Report of the SNL/NSF International Workshop on Joint Mechanics", Arlington, Virginia, 16-18 October 2006, Sandia Report 2007-7761. Sandia National Labs, Albuquerque, NM.
- [2] Mulvihill, D. M., Kartal, M. E., Olver, A. V., Nowell, D., and Hills, D. A., 2011, "Investigation of non-Coulomb friction behaviour in reciprocating sliding," *Wear*, 271(5-6), pp. 802-816.
- [3] Mulvihill, D. M., Kartal, M. E., Nowell, D., and Hills, D. A., 2011, "An elastic-plastic asperity interaction model for sliding friction," *Tribology International*, 44(12), pp. 1679-1694.
- [4] Kartal, M. E., Mulvihill, D. M., Nowell, D., and Hills, D. A., 2011, "Determination of the frictional properties of titanium and nickel alloys using the digital image correlation method," *Experimental Mechanics*, 51(3), pp. 359-371.
- [5] Kartal, M. E., Mulvihill, D. M., Nowell, D., and Hills, D. A., 2011, "Measurements of pressure and area dependent tangential contact stiffness between rough surfaces using digital image correlation," *Tribology International*, 44(10), pp. 1188-1198.
- [6] de Crevoisier, J., Swiergiel, N., Champaney, L., and Hild, F., 2012, "Identification of in situ frictional properties of bolted assemblies with digital image correlation," *Experimental Mechanics*, 52(6), pp. 561-572.
- [7] Kendall, K., and Tabor, D., 1971, "An ultrasonic study of the area of contact between stationary and sliding surfaces," *Proceedings of the Royal Society of London. Series A, Mathematical and Physical Sciences*, 323(1554), pp. 321-340.
- [8] Królikowski, J., Szczepek, J., and Witczak, Z., 1986, "High pressure in ultrasonic study of contact of solids," *Physica B+C*, 139-140, pp. 803-805.
- [9] Królikowski, J., Szczepek, J., and Witczak, Z., 1989, "Ultrasonic investigation of contact between solids under high hydrostatic pressure," *Ultrasonics*, 27(1), pp. 45-49.
- [10] Królikowski, J., and Szczepek, J., 1991, "Prediction of contact parameters using ultrasonic method," *Wear*, 148(1), pp. 181-195.
- [11] Królikowski, J., and Szczepek, J., 1993, "Assessment of tangential and normal stiffness of contact between rough surfaces using ultrasonic method," *Wear*, 160(2), pp. 253-258.
- [12] Drinkwater, B. W., Dwyer-Joyce, R. S., and Cawley, P., 1996, "A study of the interaction between ultrasound and a partially contacting solid-solid Interface," *Proceedings: Mathematical, Physical and Engineering Sciences*, 452(1955), pp. 2613-2628.

- 1
2
3
4 [13] Dwyer-Joyce, R. S., Drinkwater, B. W., and Quinn, A. M., 2001, "The use of ultrasound
5 in the investigation of rough surface interfaces," *Journal of Tribology*, 123(1), pp. 8-16.
6 [14] Baltazar, A., Rokhlin, S. I., and Pecorari, C., 2002, "On the relationship between
7 ultrasonic and micromechanical properties of contacting rough surfaces," *Journal of the*
8 *Mechanics and Physics of Solids*, 50(7), pp. 1397-1416.
9 [15] Kim, J.-Y., Baltazar, A., and Rokhlin, S. I., 2004, "Ultrasonic assessment of rough
10 surface contact between solids from elastoplastic loading-unloading hysteresis cycle," *Journal*
11 *of the Mechanics and Physics of Solids*, 52(8), pp. 1911-1934.
12 [16] Dwyer-Joyce, R. S., and Gonzalez-Valadez, M., 2004, "Ultrasonic determination of
13 normal and shear interface stiffness and the effect of Poisson's ratio", in Dalmaz, G.,
14 Lubrecht, A. A., Dawson, D., and Priest, M., eds., *Transient processes in tribology:*
15 *Proceedings of the 30th Leeds-Lyon Symposium*, Lyon, France, Sept 2nd - 5th.
16 [17] Gonzalez-Valadez, M., Baltazar, A., and Dwyer-Joyce, R. S., 2010, "Study of interfacial
17 stiffness ratio of a rough surface in contact using a spring model," *Wear*, 268(3-4), pp. 373-
18 379.
19 [18] Tattersall, H. G., 1973, "The ultrasonic pulse-echo technique as applied to adhesion
20 testing," *Journal of Applied Physics D: Applied Physics*, 6(7), pp. 819-832.
21 [19] Rose, J. H., 1989, "Ultrasonic reflectivity of diffusion bonds" in *Review of progress in*
22 *quantitative NDE*, Thompson D.O and Chimenti D.E., eds., vol 8B, pp. 1925-1931.
23 [20] TiMetal 6-4 datasheet, 2000, Titanium Metals Corporation (TIMET), Hartford, CT,
24 USA.
25 [21] PixeLINK PL-B741U monochrome camera data sheet, 2009, PixeLINK, Ottawa,
26 Canada.
27 [22] Questar QM1 Long Distance Microscope Datasheet, Questar Corporation, New Hope,
28 PA, USA.
29 [23] Video Gauge User Guide, 2009, Imetrum Limited, Bristol, UK.
30 [24] Schreier, H. W., Braasch, J. R., and Sutton, M. A., 2000, "Systematic errors in digital
31 image correlation caused by intensity interpolation," *Optical Engineering*, 39(11), pp. 2915-
32 2921.
33 [25] Knauss, W. G., Chasiotis, I., and Huang, Y., 2003, "Mechanical measurements at the
34 micron and nanometer scales," *Mechanics of Materials*, 35(3-6), pp. 217-231.
35 [26] Pan, B., Qian, K., Xie, H., and Asundi, A., 2009, "Two-dimensional digital image
36 correlation for in-plane displacement and strain measurement: a review," *Measurement*
37 *Science and Technology*, 20(6), pp. 1-17.
38 [27] Hild, F., and Roux, S., 2006, "Digital image correlation: from displacement
39 measurement to identification of elastic properties – a review," *Strain*, 42(2), pp. 69-80.
40 [28] McFarlane, J. S., and Tabor, D., 1950, "Relation between friction and adhesion,"
41 *Proceedings of the Royal Society of London. Series A. Mathematical and Physical Sciences*,
42 202(1069), pp. 244-253.
43 [29] DaVis StrainMaster 2D Software Product Manual, 2010, LaVision GmbH, Goettingen,
44 Germany.
45 [30] Mindlin, R. D., 1949, "Compliance of elastic bodies in contact," *Journal of Applied*
46 *Mechanics.*, 16, p. 259.
47 [31] Greenwood, J. A., and Williamson, J. B. P., 1966, "Contact of nominally flat surfaces,"
48 *Proceedings of the Royal Society of London. Series A, Mathematical and Physical Sciences*,
49 295(1442), pp. 300-319.
50 [32] Johnson, K. L., 1955, "Surface interaction between elastically loaded bodies under
51 tangential forces," *Proceedings of the Royal Society of London. Series A, Mathematical and*
52 *Physical Sciences*, 230(1183), pp. 531-548.
53
54
55
56
57
58
59
60
61
62
63
64
65

1
2
3
4
5
6
7
8
9
10
11
12
13
14
15
16
17
18
19
20
21
22
23
24
25
26
27
28
29
30
31
32
33
34
35
36
37
38
39
40
41
42
43
44
45
46
47
48
49
50
51
52
53
54
55
56
57
58
59
60
61
62
63
64
65

[33] O'Connor, J. J., and Johnson, K. L., 1963, "The role of surface asperities in transmitting tangential forces between metals," *Wear*, 6(2), pp. 118-139.

[34] Berthoud, P., and Baumberger, T., 1998, "Shear stiffness of a solid-solid multicontact interface," *Proceedings: Mathematical, Physical and Engineering Sciences*, 454(1974), pp. 1615-1634.

[35] Shi, X., and Polycarpou, A. A., 2005, "Measurement and modeling of normal contact stiffness and contact damping at the meso scale," *Journal of Vibration and Acoustics*, 127(1), pp. 52-60.

[36] Campañá, C., Persson, B. N. J., and Müser, M. H., 2011, "Transverse and normal interfacial stiffness of solids with randomly rough surfaces," *Journal of Physics: Condensed Matter*, 23(8), pp. 1-9.

[37] Sevostianov, I., and Kachanov, M., 2008, "Contact of rough surfaces: A simple model for elasticity, conductivity and cross-property connections," *Journal of the Mechanics and Physics of Solids*, 56(4), pp. 1380-1400.

[38] Proprentner, D., 2012, PhD thesis, Imperial College London.

TABLES

Table 1: Mechanical properties and chemical composition of Ti-6Al-4V.

	Poisson's ratio	0.2% Yield stress (MPa)	Chemical composition (wt. %)							
			Al	V	N	C	O	Fe	H	Ti
115	0.31	1000	5.5-6.8	3.5-4.5	0-0.05	0-0.08	0-0.2	0-0.4	0-0.02	Bal.

Table 2: Outline of the testing programme.

Test No.	Contact area (mm ²)	Loading sequence	Measurement technique and parameter measured
1 & 2	80	$p_m = \text{constant} = 70 \text{ MPa}$, Q then increased	DIC (for κ_t) + Ultrasound (for κ_t and κ_n)
3 ¹ & 4	80	$Q = \text{constant} = 0$, p_m increased to 200 MPa	DIC (for κ_n) + Ultrasound (for κ_t and κ_n)
5	80	p_m increased to 70 MPa,	Ultrasound only (for κ_t and κ_n)
6	80	p_m increased to 200 MPa	Ultrasound only (for κ_t and κ_n)
7 & 8	50	$p_m = \text{constant} = 70 \text{ MPa}$, Q then increased	DIC (for κ_t) + Ultrasound (for κ_t and κ_n)
9 & 10	50	$Q = \text{constant} = 0$, p_m increased to 200 MPa	DIC (for κ_n) + Ultrasound (for κ_t and κ_n)

¹ When p_m reached 200 MPa, tangential load Q was then applied and κ_t was measured by DIC.

Table 3: Comparison of the DIC and ultrasound measurement techniques for tangential contact stiffness measured at $p_m = 70$ MPa and $Q = 0$. Distances between measurement points for calculation of DIC relative displacements were: 137, 145, 102, and 142 μm for tests 1, 2, 7, and 8 respectively.

Test No.	Contact area (mm^2)	Tangential contact stiffness, κ_t (kN/mm^3)	
		DIC	Ultrasound
1	80	37	68
2	80	45	47
3	80	-	105
4	80	-	147
5	80	-	98
6	80	-	81
7	50	35	224
8	50	37	101
9	50	-	114
10	50	-	42

Table 4: Comparison of the DIC and ultrasound measurement techniques for normal contact stiffness measured at $p_m = 70$ MPa and $Q = 0$. Initial distances (before loading) between measurement points for calculation of DIC relative displacements were: 126, 135, 111, and 150 μm for Tests 3, 4, 9, and 10, respectively.

Test No.	Contact area (mm^2)	Normal contact stiffness, κ_n (kN/mm^3)	
		DIC	Ultrasound
1	80	-	252
2	80	-	253
3	80	101	448
4	80	80	233
5	80	-	220
6	80	-	366
7	50	-	265
8	50	-	262
9	50	73	236
10	50	56	140

FIGURES

Figure 1: Schematic diagram illustrating the quasi-static spring model for ultrasound reflection from rough interfaces.

Figure 2: Schematic diagram of the specimen and pads shown with accompanying local test setup for combined DIC–ultrasound testing.

Figure 3: Photograph of a specimen in contact with two instrumented pads.

Figure 4: Photograph of the Dartec servo-hydraulic tensile testing machine showing various features of the test setup including the camera and Questar microscope used for obtaining digital images.

Figure 5: A sample digital image of the pad-specimen interface from one of the tests showing the targets (T1 – T20) used for DIC analysis with the Imetrum Video Gauge software. (image dimensions: 1 mm × 1.3 mm)

Figure 6: Absolute displacement profile of points initially lying on the central normal to the contact patch recorded in Test 1 when $Q/fP = 0.48$ as the tangential load is increased.

Figure 7: Plots of tangential force, Q , versus relative tangential displacement derived from DIC for: (a) Test 1, (b) Test 2, (c) Test 7, and (d) Test 8. Distances between the measurement points used for calculation of relative displacement were: 137 μm for (a), 145 μm for (b), 102 μm for (c), and 142 μm for (d). Rational curve fits to the data are also shown. $p_m = 70$ MPa in each case.

Figure 8: Comparison of DIC (left) with ultrasound (right) tangential contact stiffness (per unit area). Variation with tangential load for: (a) Test 1, (b) Test 2, (c) Test 7, and (d) Test 8. Distances between measurement points for calculation of relative displacement for DIC were: 137 μm for (a), 145 μm for (b), 102 μm for (c), and 142 μm for (d). $p_m = 70$ MPa.

Figure 9: Schematic diagram showing the difference between tangential contact stiffness derived from DIC (the tangent stiffness) with that derived from ultrasound (the local unloading stiffness).

Figure 10: Variation of normal contact stiffness (per unit area) measured by ultrasound with tangential load in Tests 1, 2, 7, and 8. Mean normal contact pressure is 70 MPa in each test.

1
2
3
4 Figure 11: Plots of normal force, P , versus relative normal displacement derived from DIC
5 for: (a) Test 3, (b) Test 4, (c) Test 9, and (d) Test 10. Initial distances (at $P = 0$) between
6 measurement points for calculation of relative displacement were: 126 μm for (a), 135 μm for
7 (b), 111 μm for (c), and 150 μm for (d). Rational polynomial curve fits to the data are also
8 shown.
9

10
11
12 Figure 12: Comparison of DIC with ultrasound for the variation of normal contact stiffness
13 (per unit area) with normal contact pressure: (a) Test 4, and (b) Test 9. Initial distance
14 between measurement points for DIC (i.e. before loading) were 135 μm for (a) and 111 μm
15 for (b).
16
17

18
19 Figure 13: Variation of tangential contact stiffness per unit area (ultrasound only) with p_m for
20 Tests 3, 4, 6, & 9.
21
22

23
24 Figure 14: Comparison of contact stiffness (per unit area) derived from an elastic ‘smooth
25 contact’ finite element model [4] with that derived from DIC: (a) tangential contact stiffness
26 (DIC tangent stiffness at $Q = 0$ from Test 1 and Test 3), and (b) normal contact stiffness (DIC
27 tangent stiffness from Test 3). An ‘isolated interface stiffness’ for the DIC results at the 70
28 MPa normal pressure is also given in (a) and (b). Contact area: 80 mm^2 in both cases.
29
30
31
32
33
34
35
36
37
38
39
40
41
42
43
44
45
46
47
48
49
50
51
52
53
54
55
56
57
58
59
60
61
62
63
64
65

1
2
3
4
5
6
7
8
9
10
11
12
13
14
15
16
17
18
19
20
21
22
23
24
25
26
27
28
29
30
31
32
33
34
35
36
37
38
39
40
41
42
43
44
45
46
47
48
49
50
51
52
53
54
55
56
57
58
59
60
61
62
63
64
65

Figure 1

[Click here to download Figure: Fig01.pdf](#)

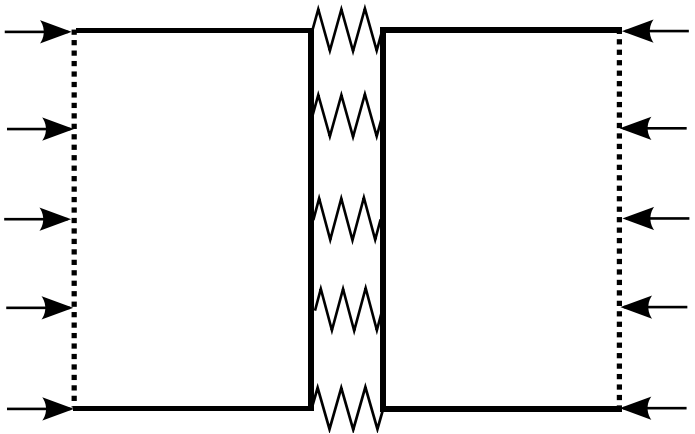
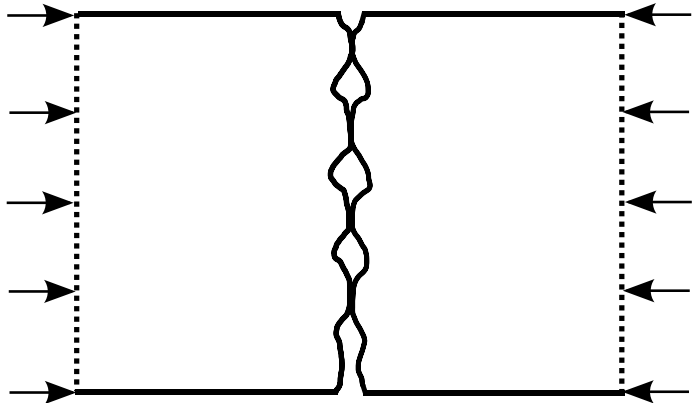
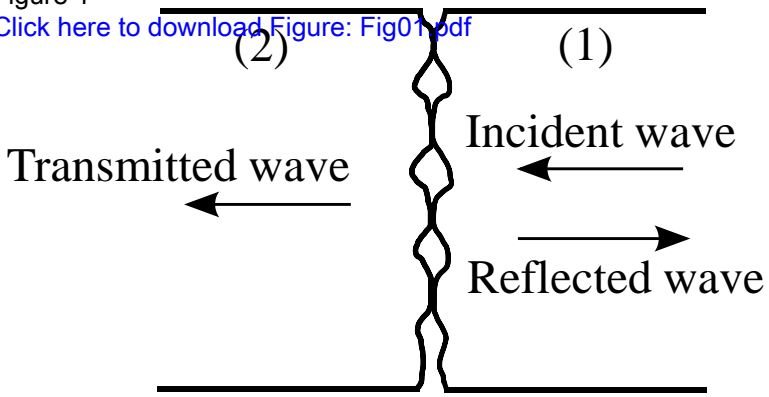


Figure 2

[Click here to download Figure: Fig02.pdf](#)

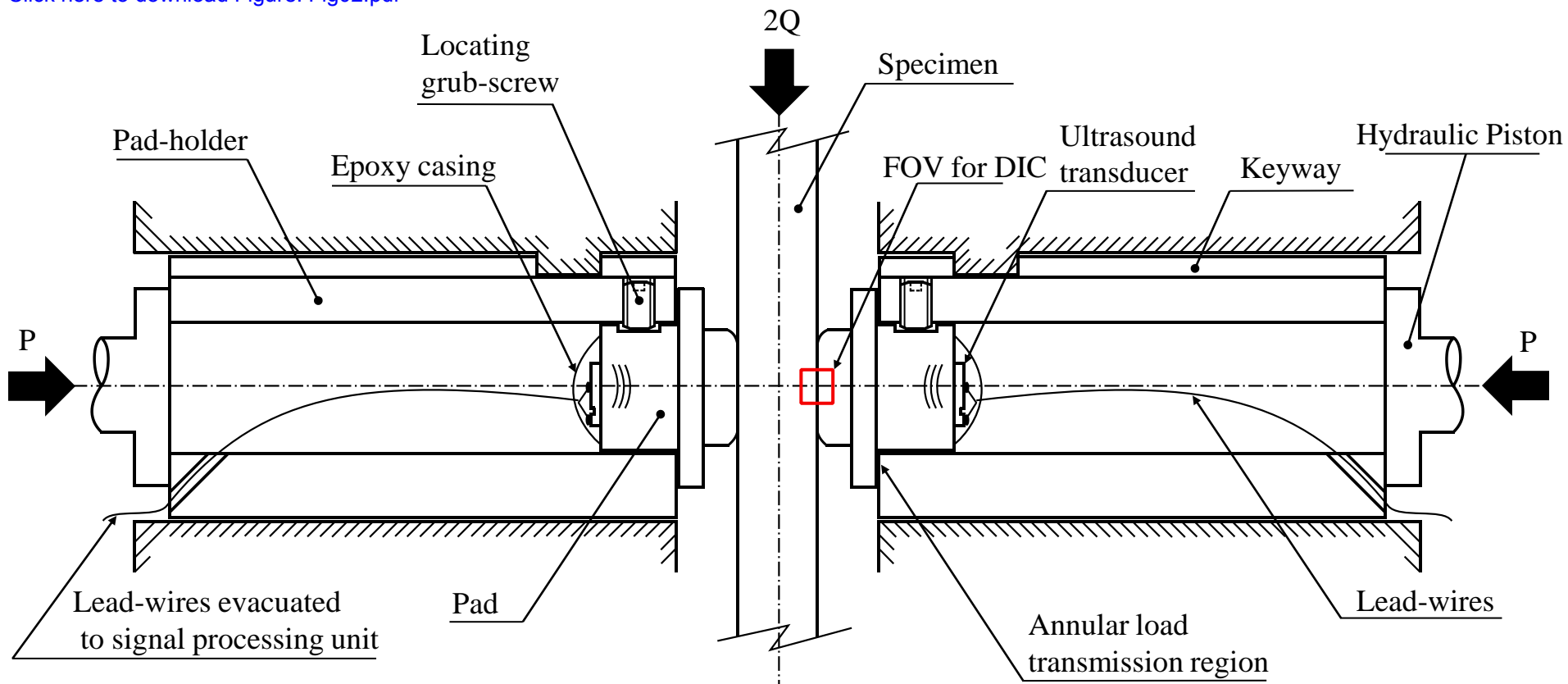


Figure 3
[Click here to download high resolution image](#)

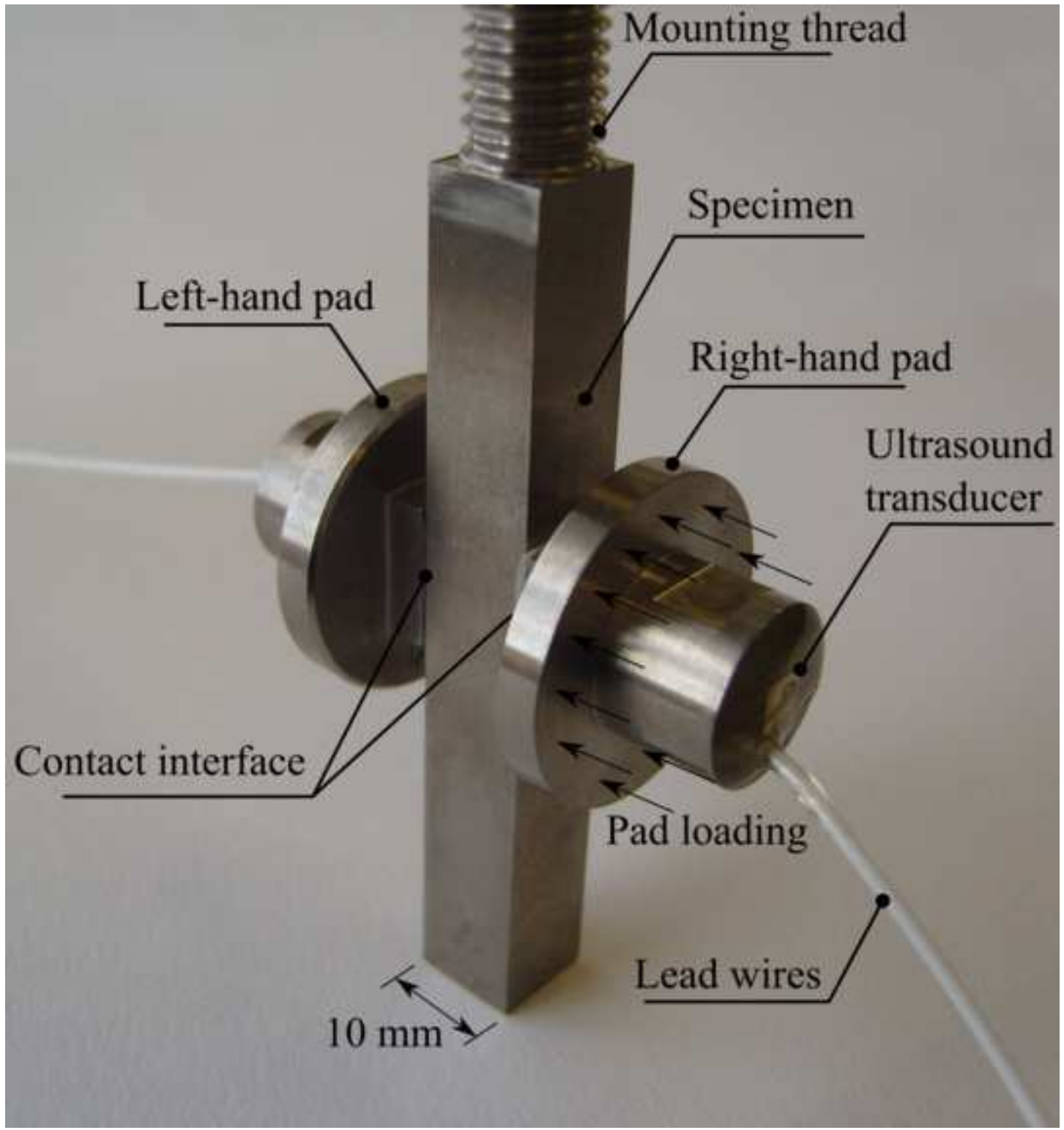


Figure 4

[Click here to download high resolution image](#)



Figure 5
[Click here to download high resolution image](#)



Figure 6
[Click here to download Figure: Fig06.pdf](#)

Distance from interface (μm)

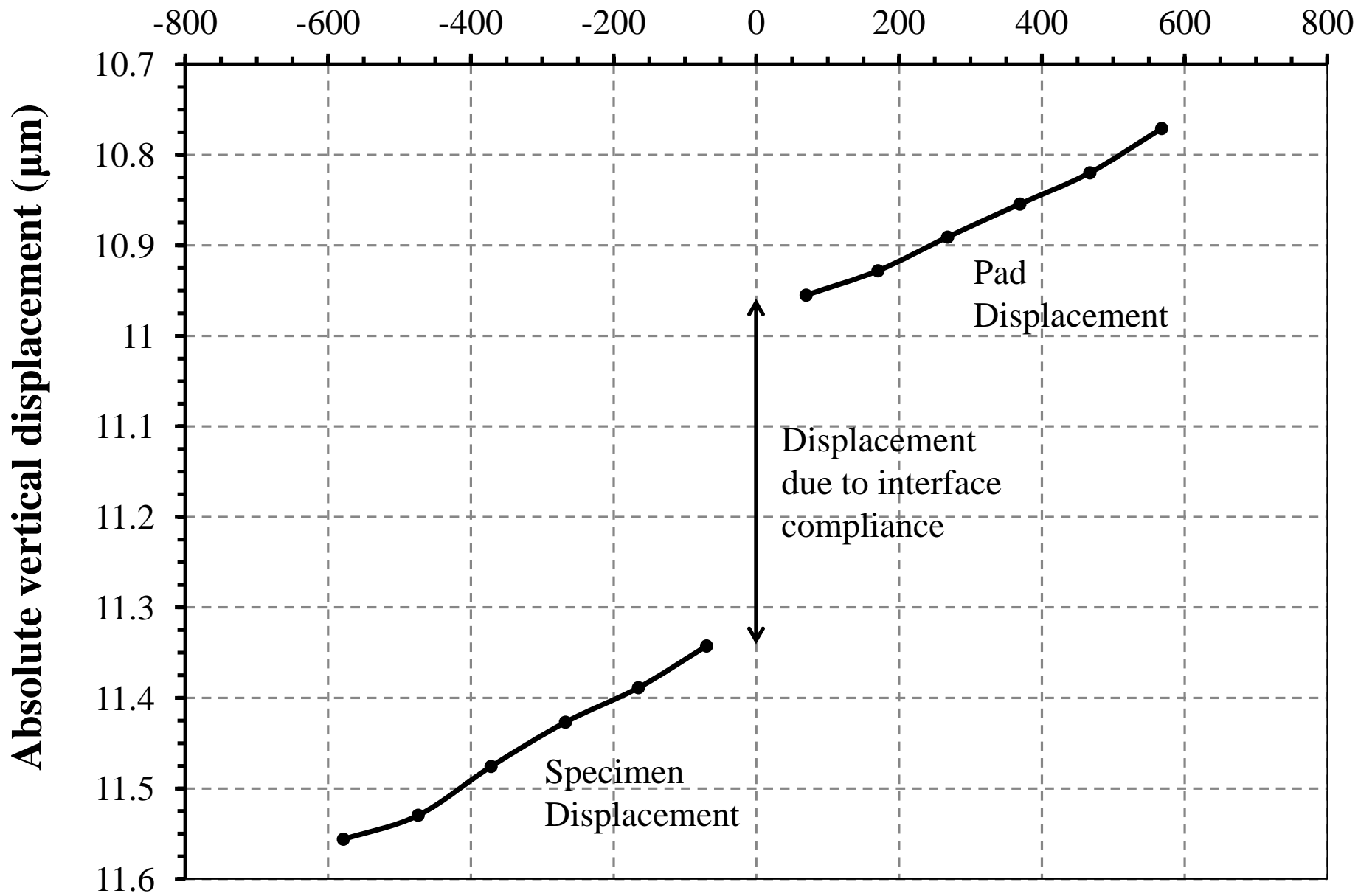


Figure 7a
[Click here to download Figure: Fig07a.pdf](#)

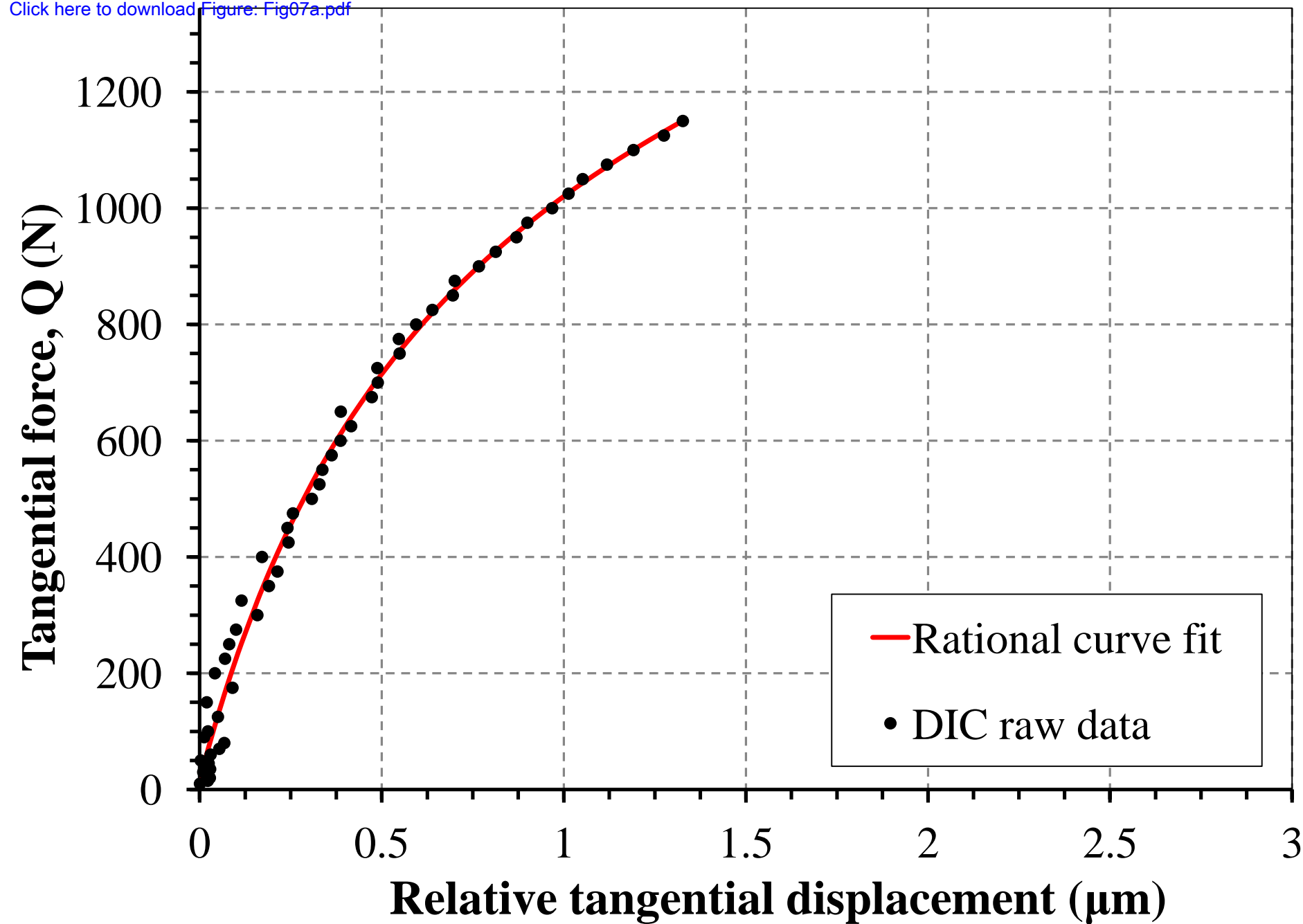


Figure 7b
[Click here to download Figure: Fig07b.pdf](#)

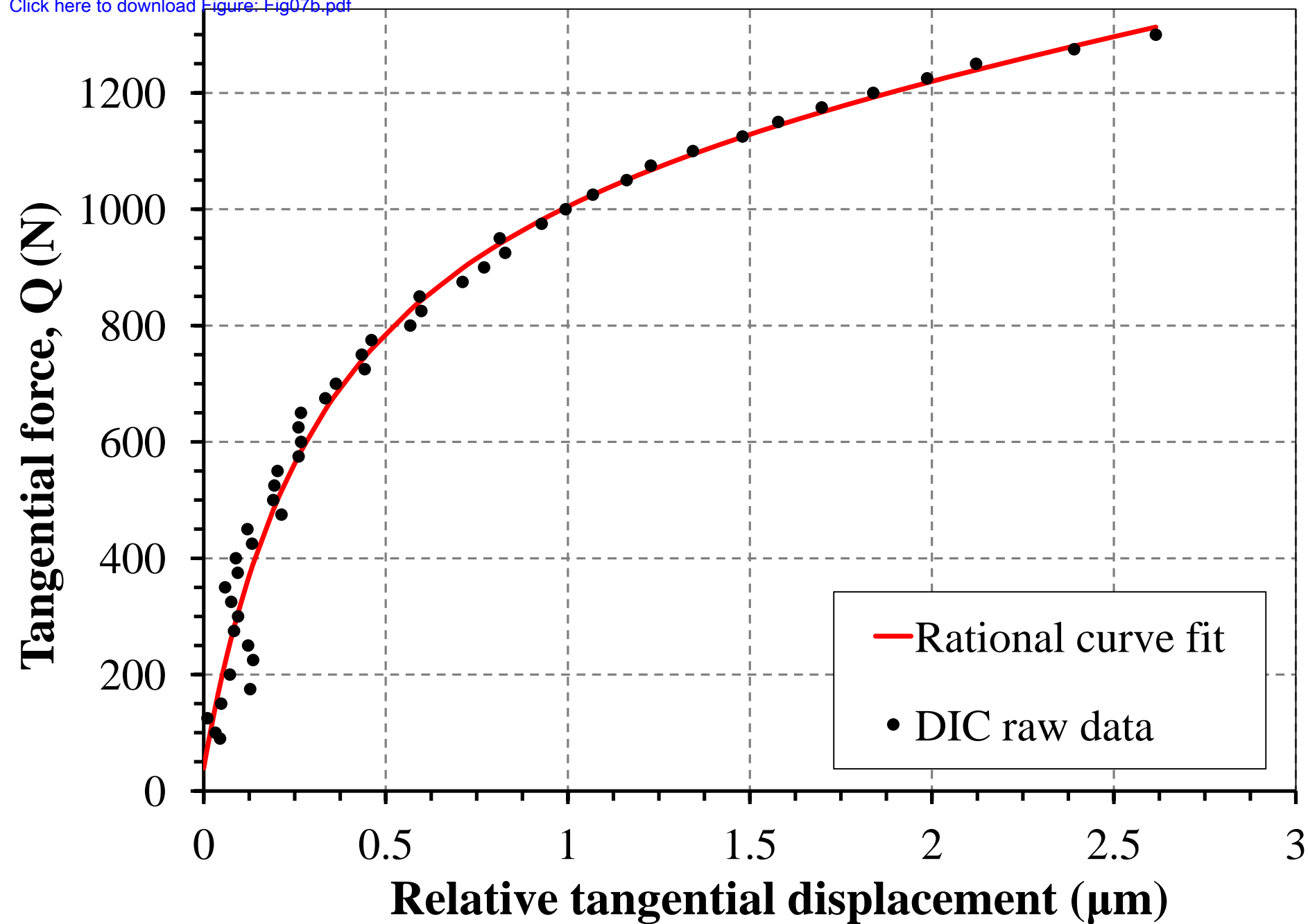


Figure 7c
[Click here to download Figure: Fig07c.pdf](#)

Tangential force, Q (N)

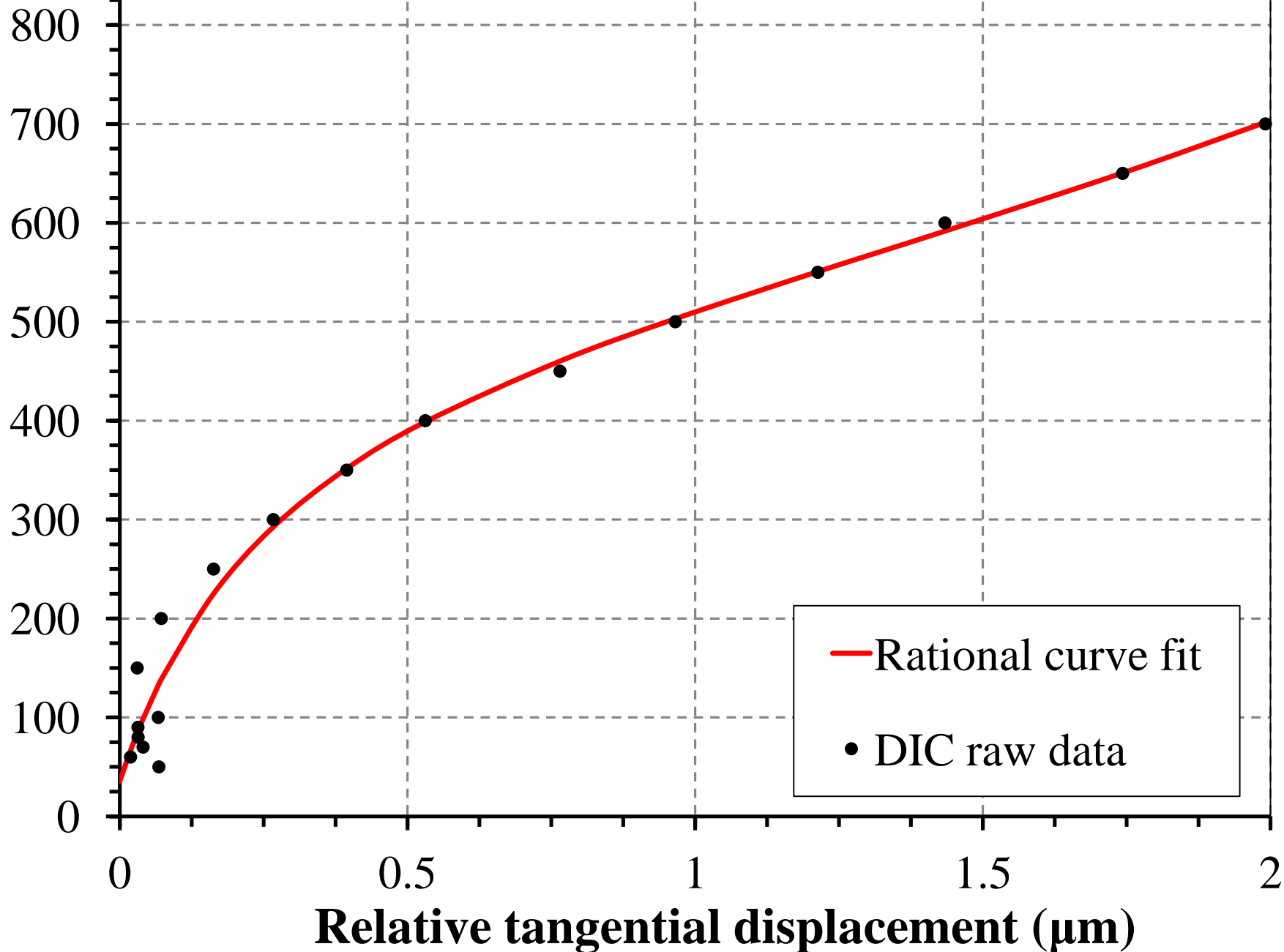
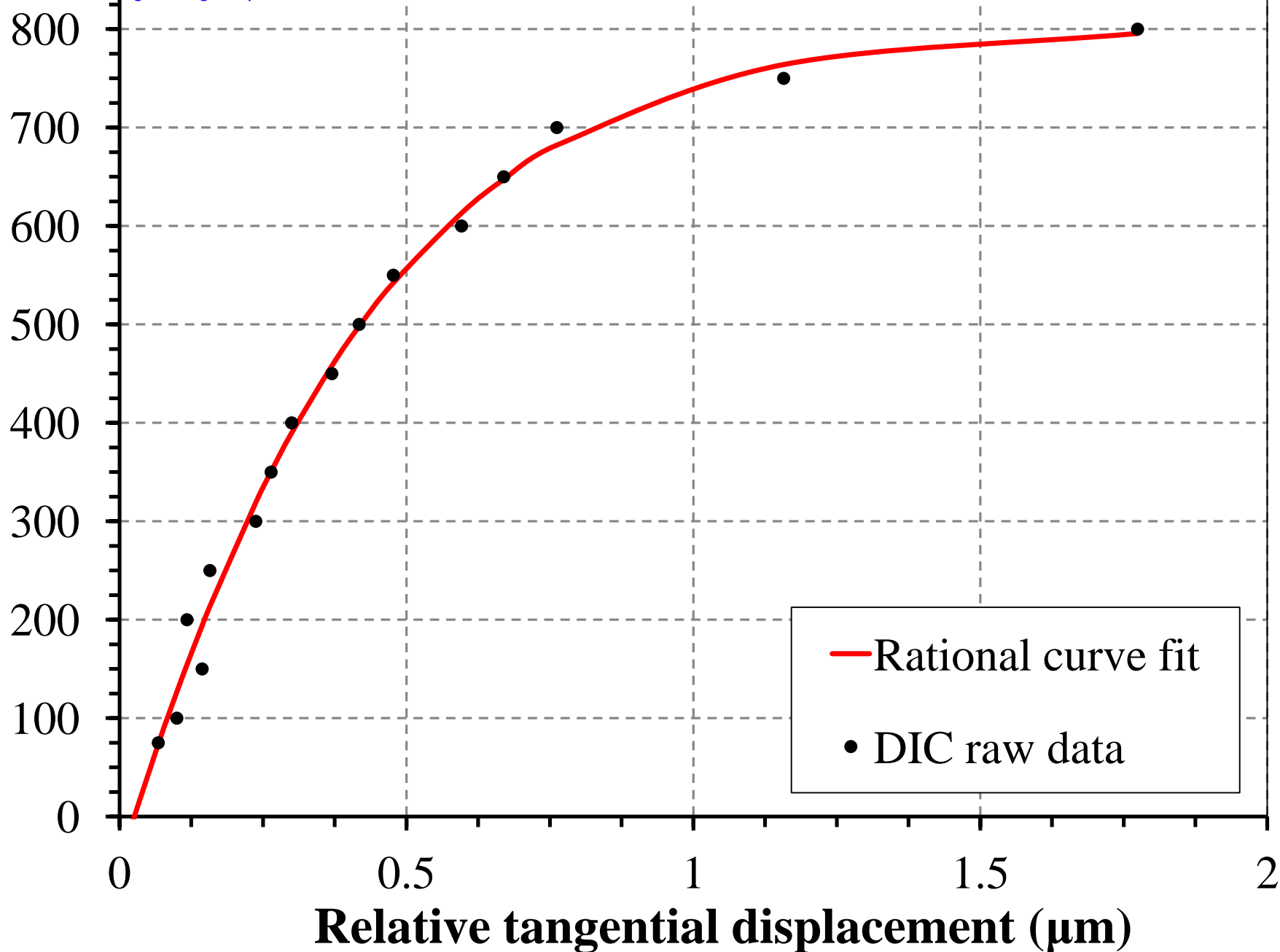
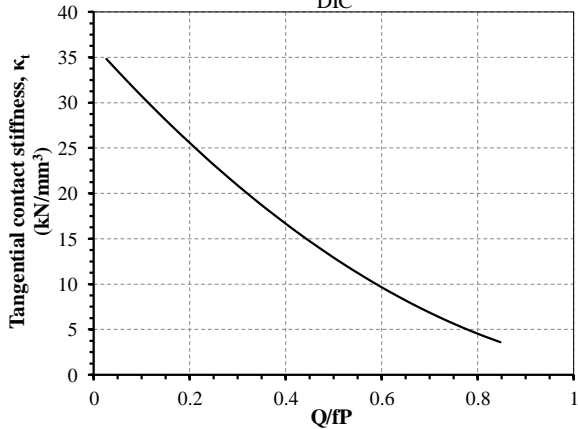


Figure 7d
[Click here to download Figure: Fig07d.pdf](#)

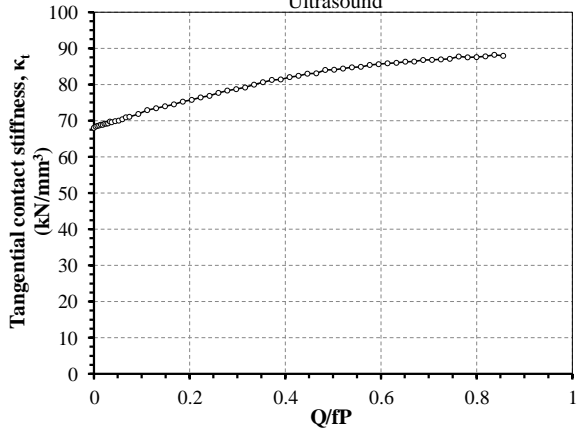
Tangential force, Q (N)

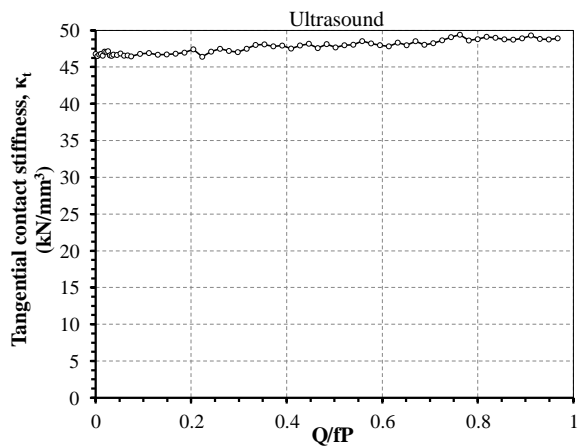
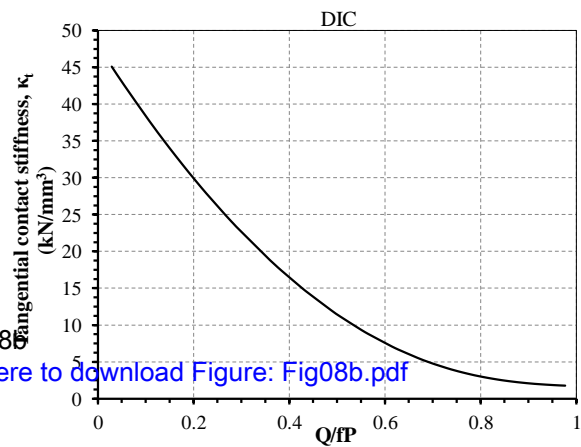


DIC



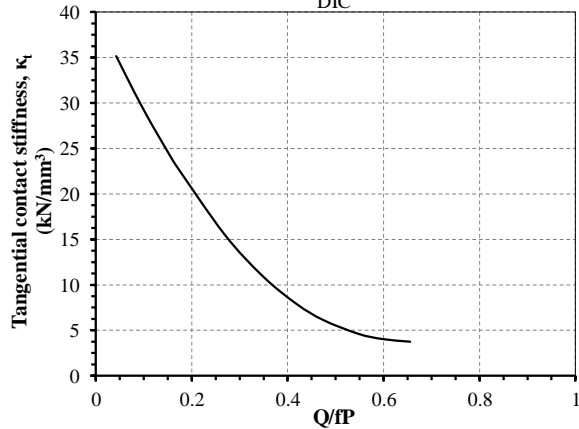
Ultrasound



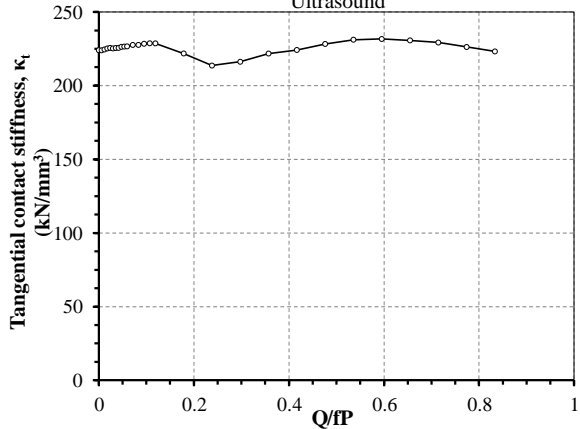


Click here to download Figure: Fig08b.pdf

DIC



Ultrasound



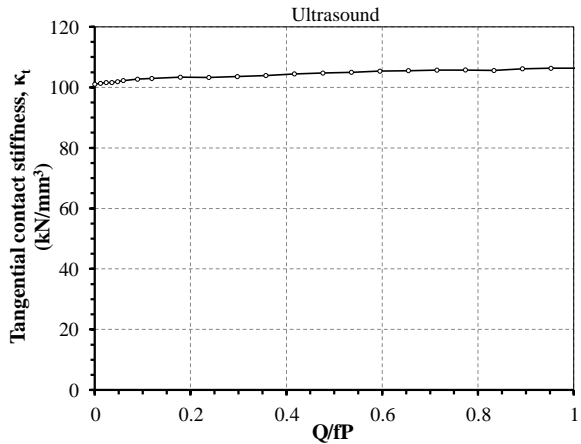
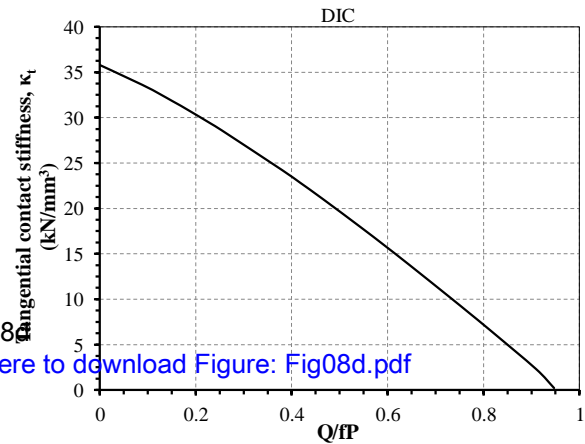


Figure 9
[Click here to download Figure: Fig09.pdf](#)

Tangential Force, Q

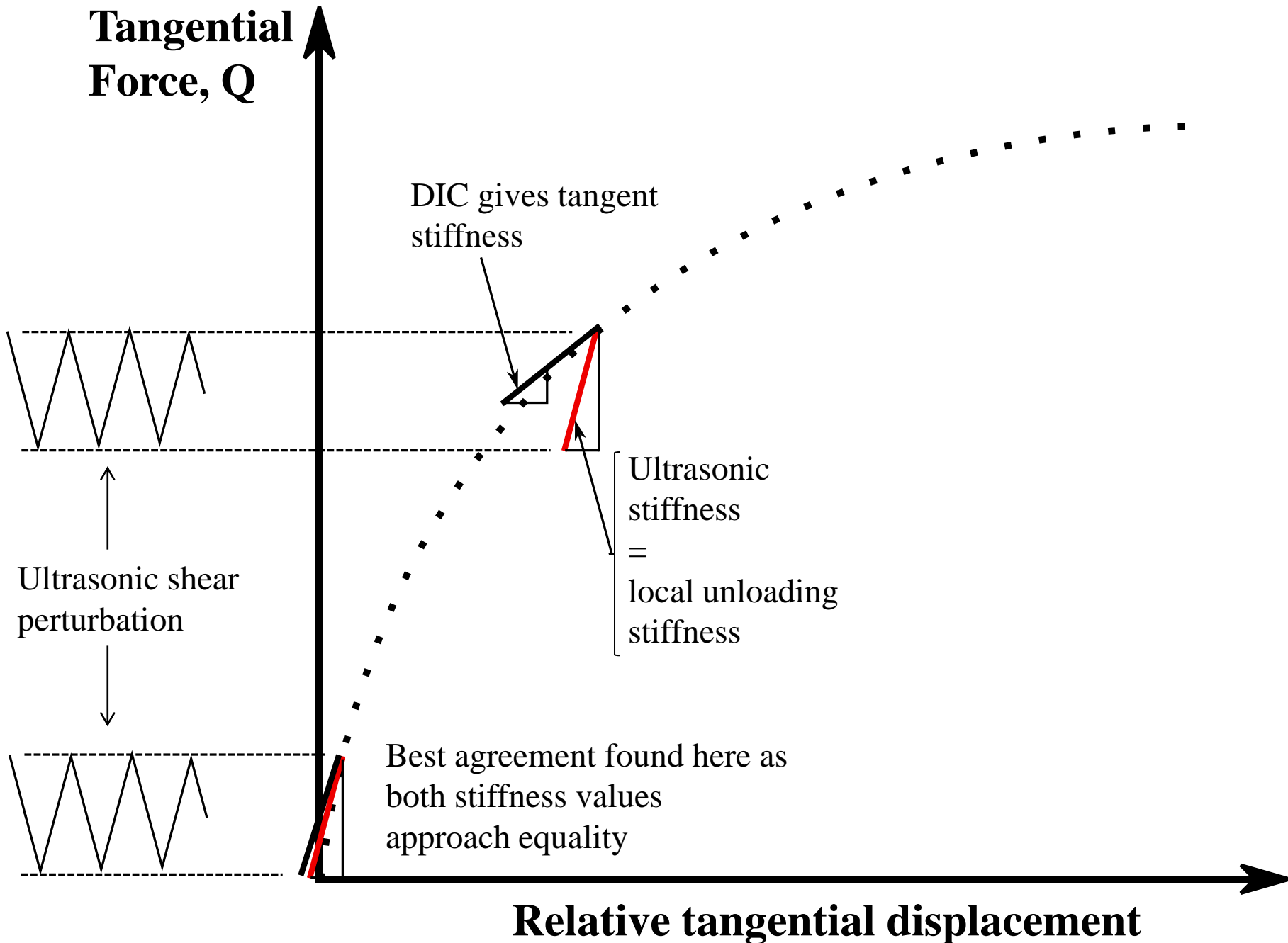


Figure 10
[Click here to download Figure: Fig10.pdf](#)

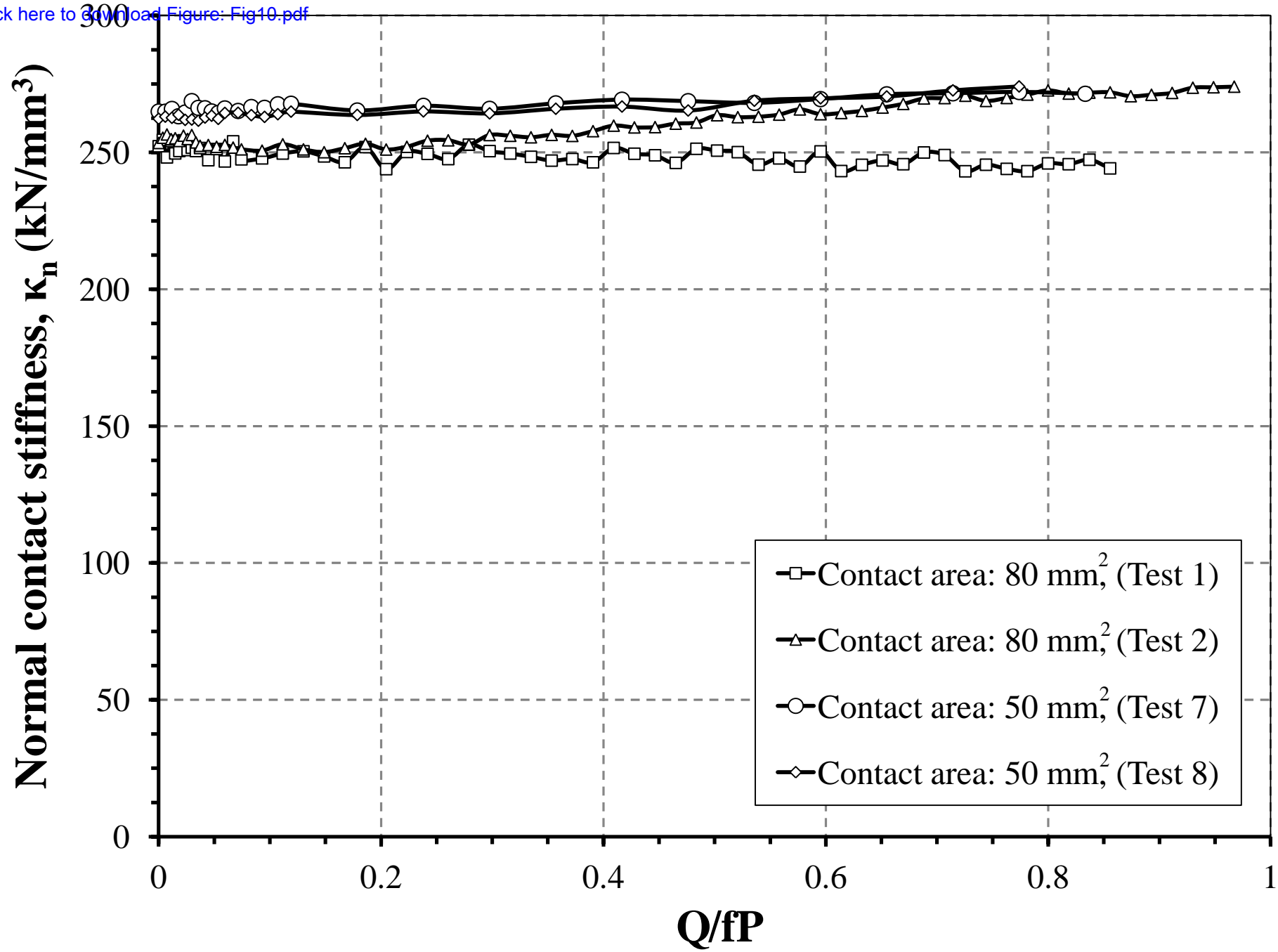


Figure 11a
[Click here to download Figure: Fig11a.pdf](#)

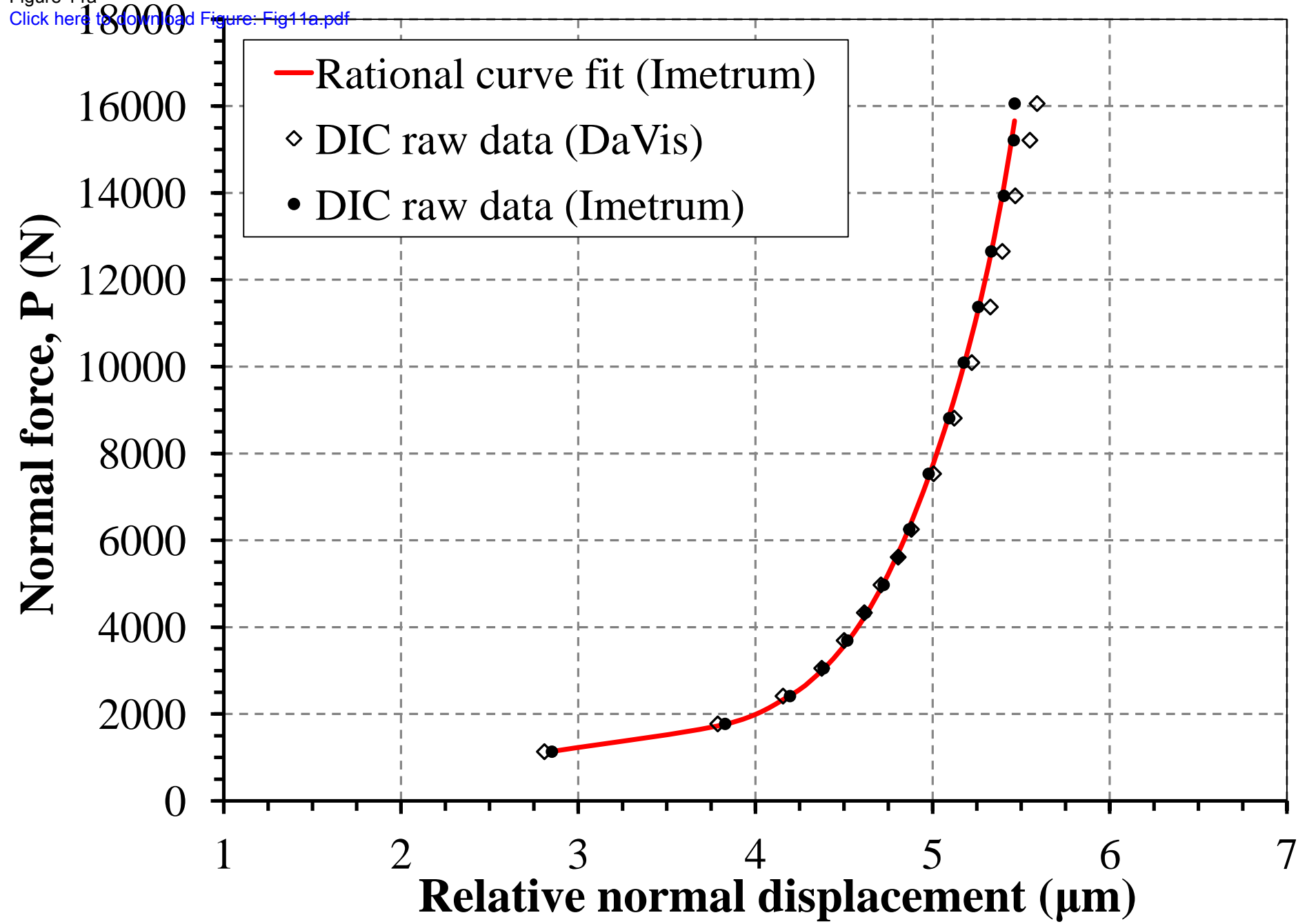


Figure 11b
[Click here to download Figure: Fig11b.pdf](#)

Normal force, P (N)

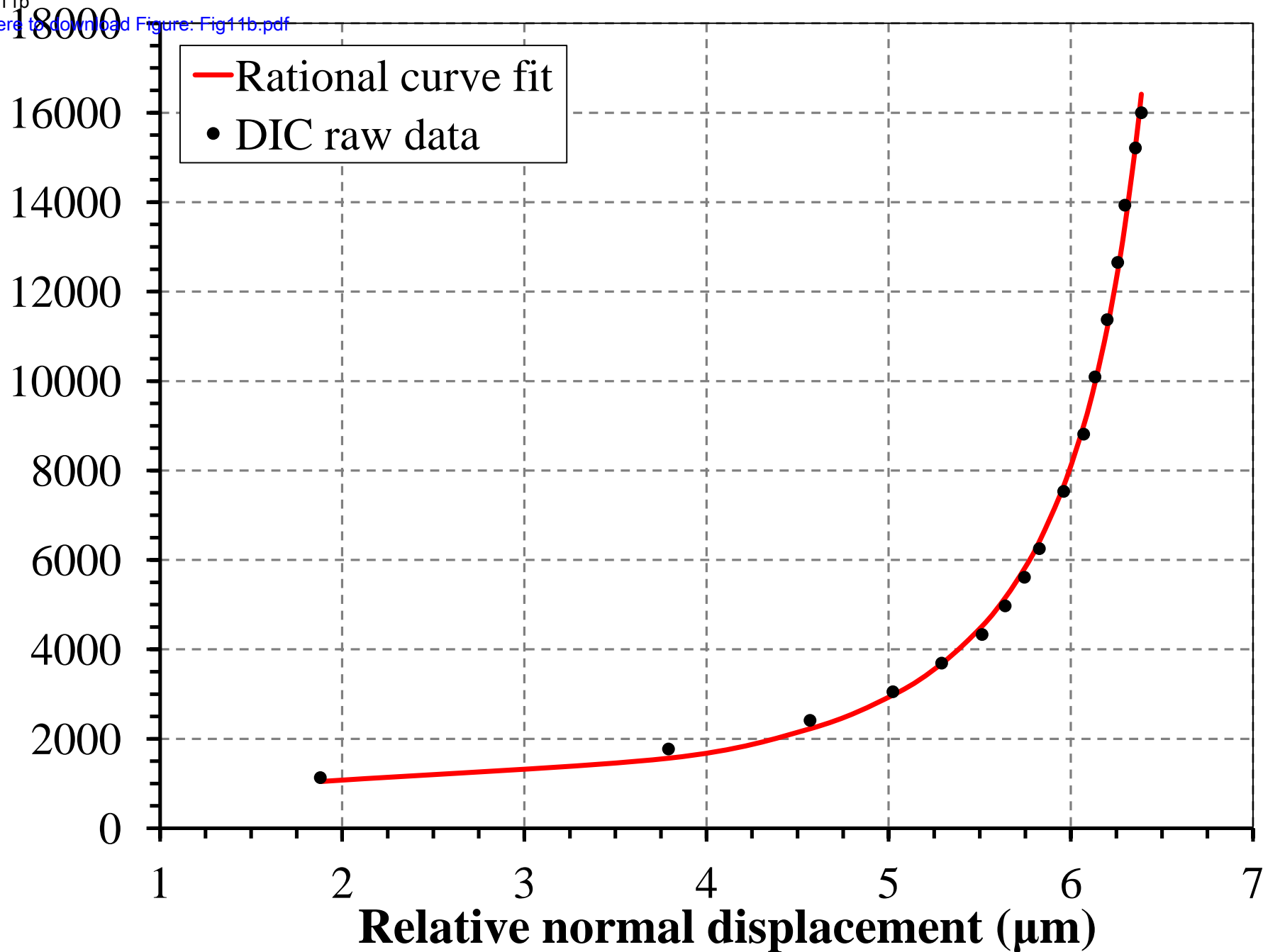


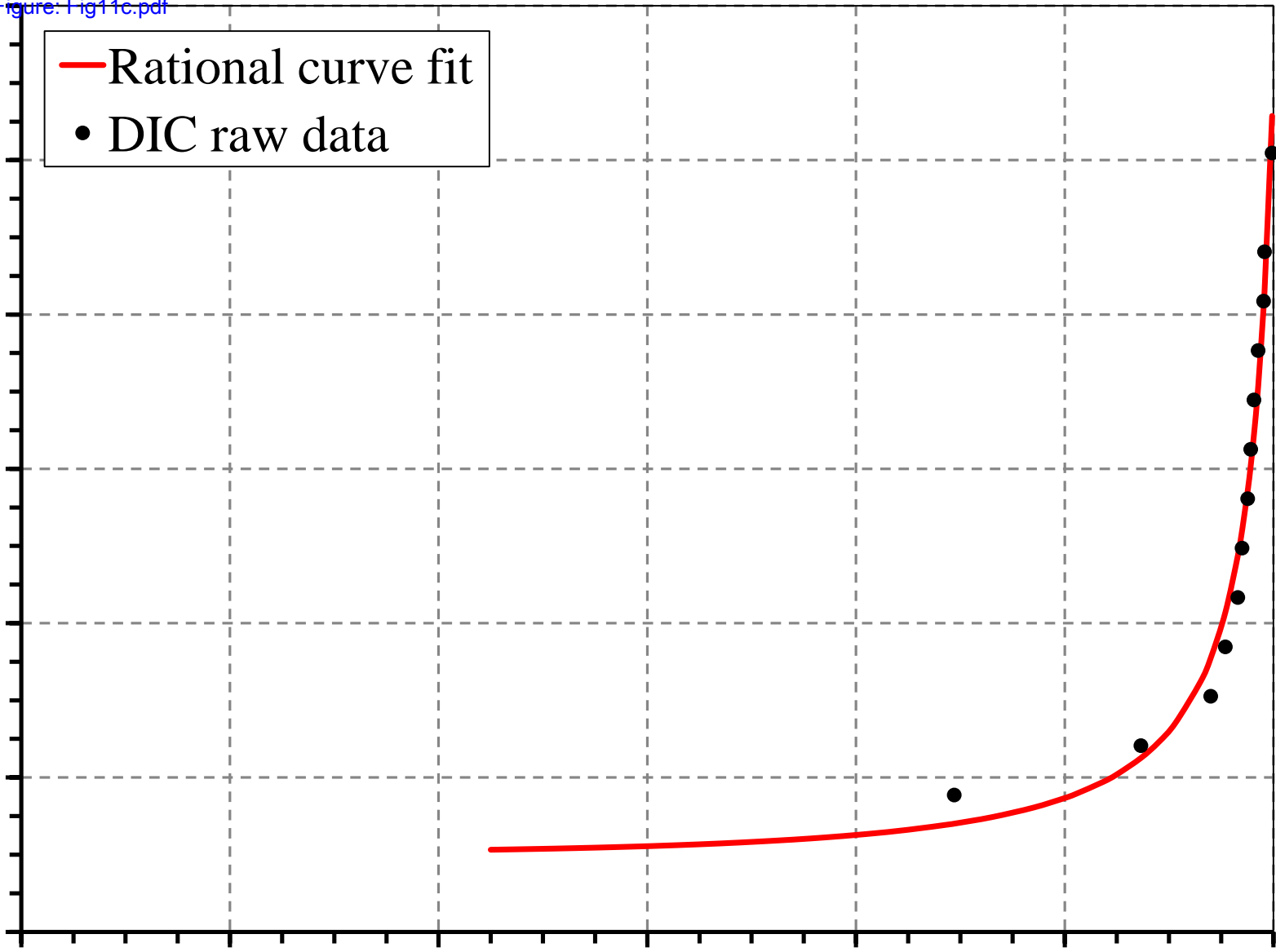
Figure 11c
[Click here to download Figure: Fig11c.pdf](#)

Normal force, P (N)

12000
10000
8000
6000
4000
2000
0

— Rational curve fit
• DIC raw data

0 2 4 6 8 10 12
Relative normal displacement (μm)



Normal force, P (N)

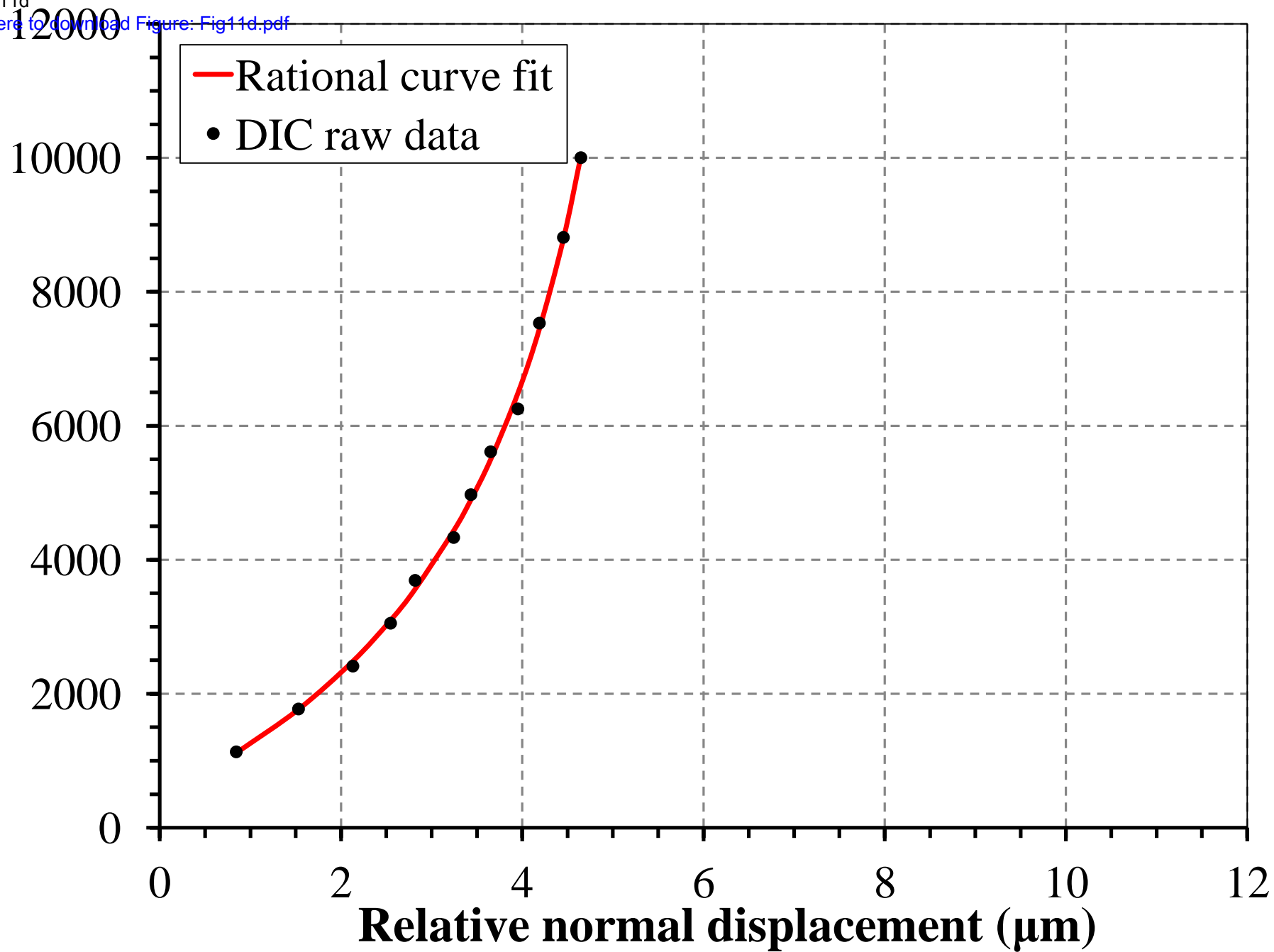


Figure 12a
[Click here to download Figure: Fig12a.pdf](#)

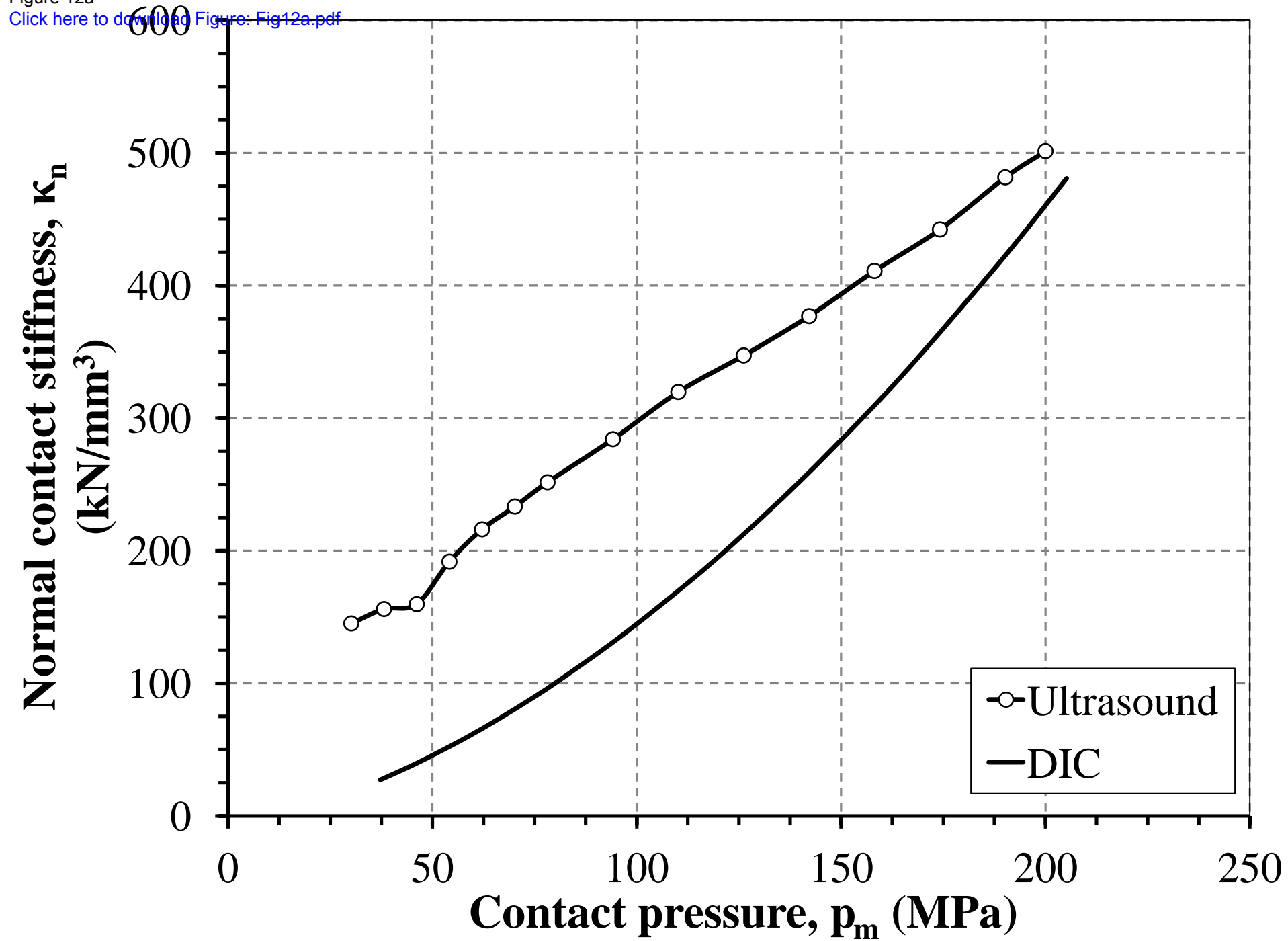


Figure 12b
[Click here to download Figure: Fig12b.pdf](#)

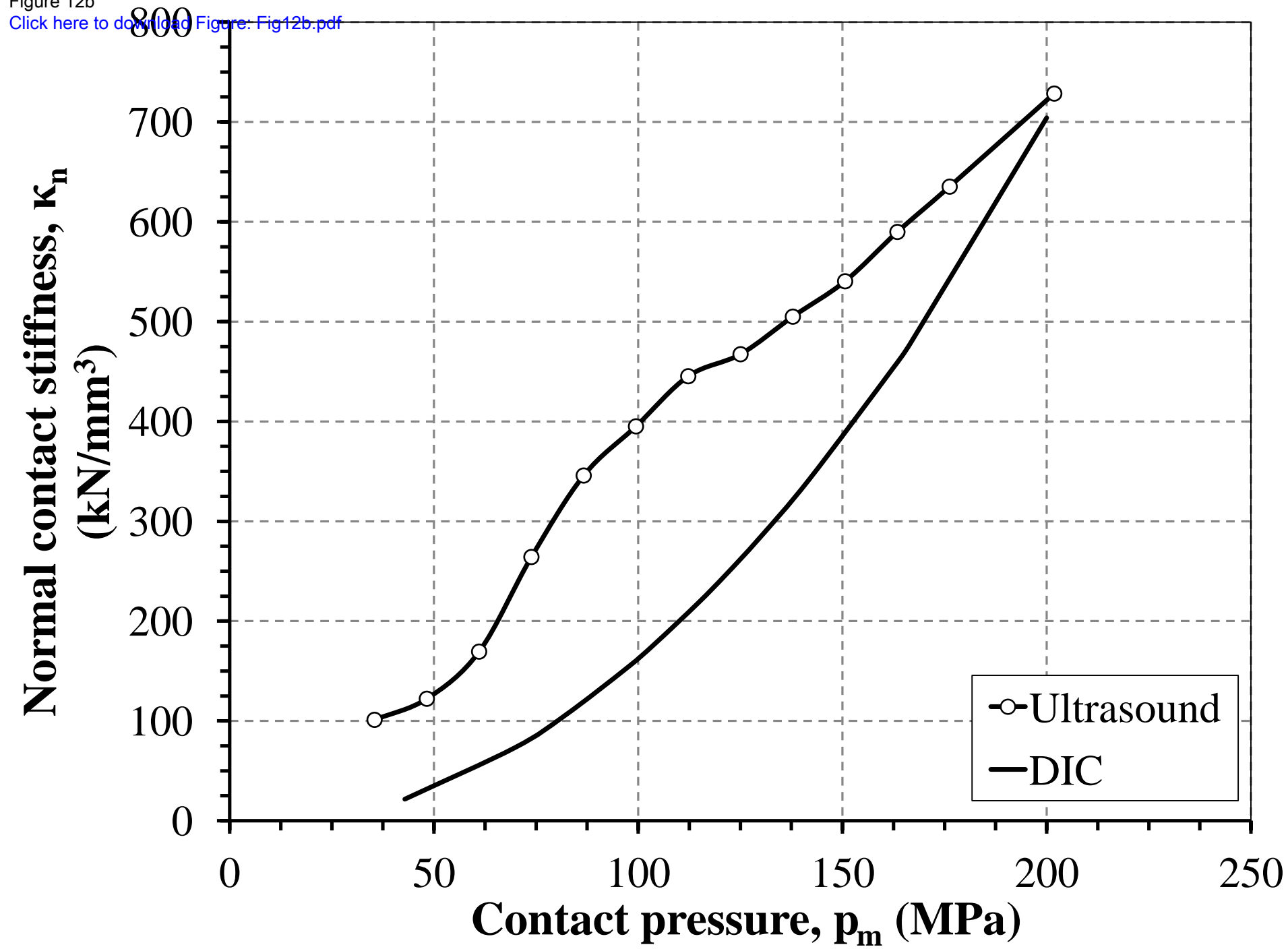


Figure 13
[Click here to download Figure: Fig13.pdf](#)

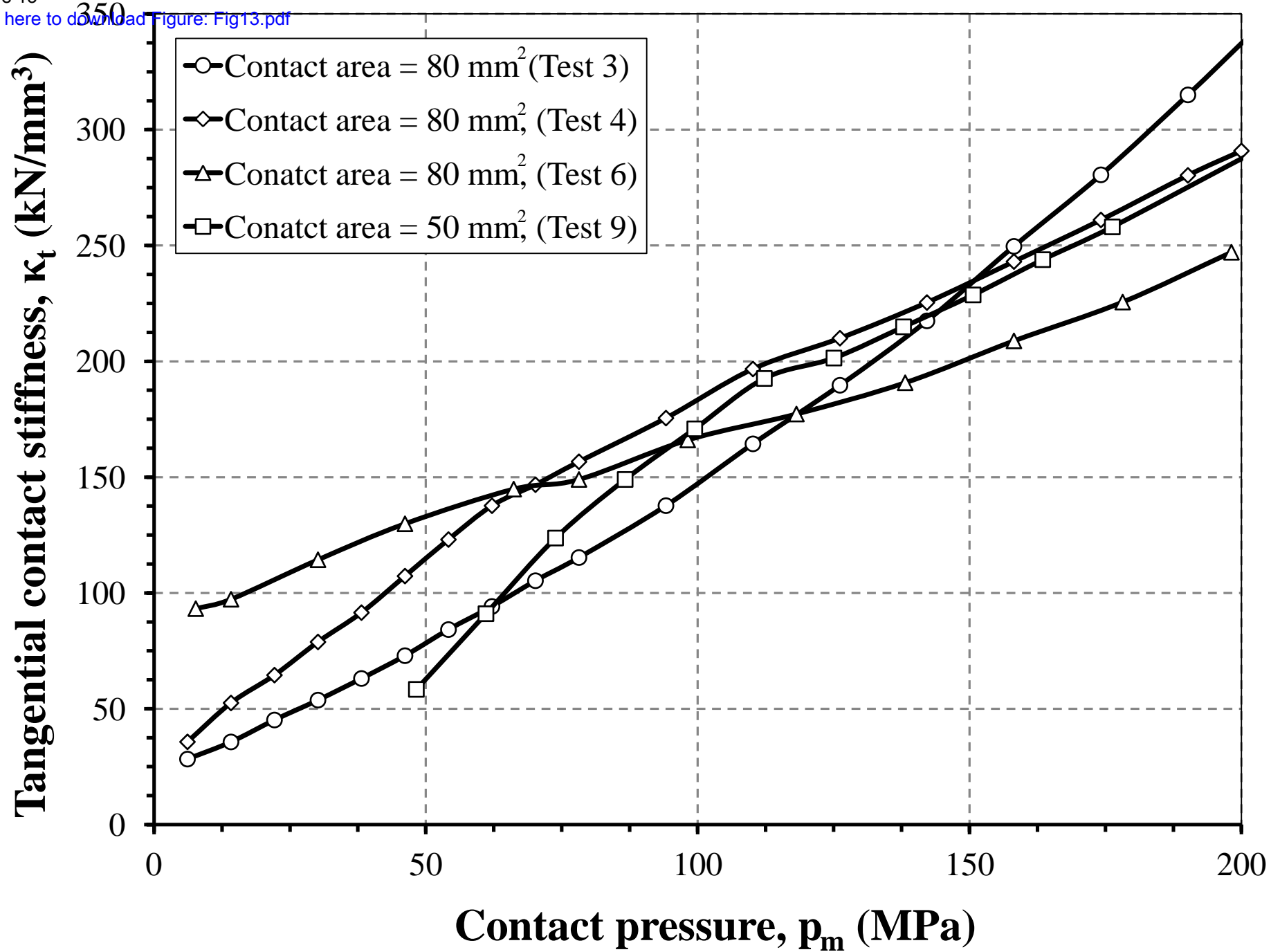


Figure 14a
[Click here to download Figure: Fig14a.pdf](#)

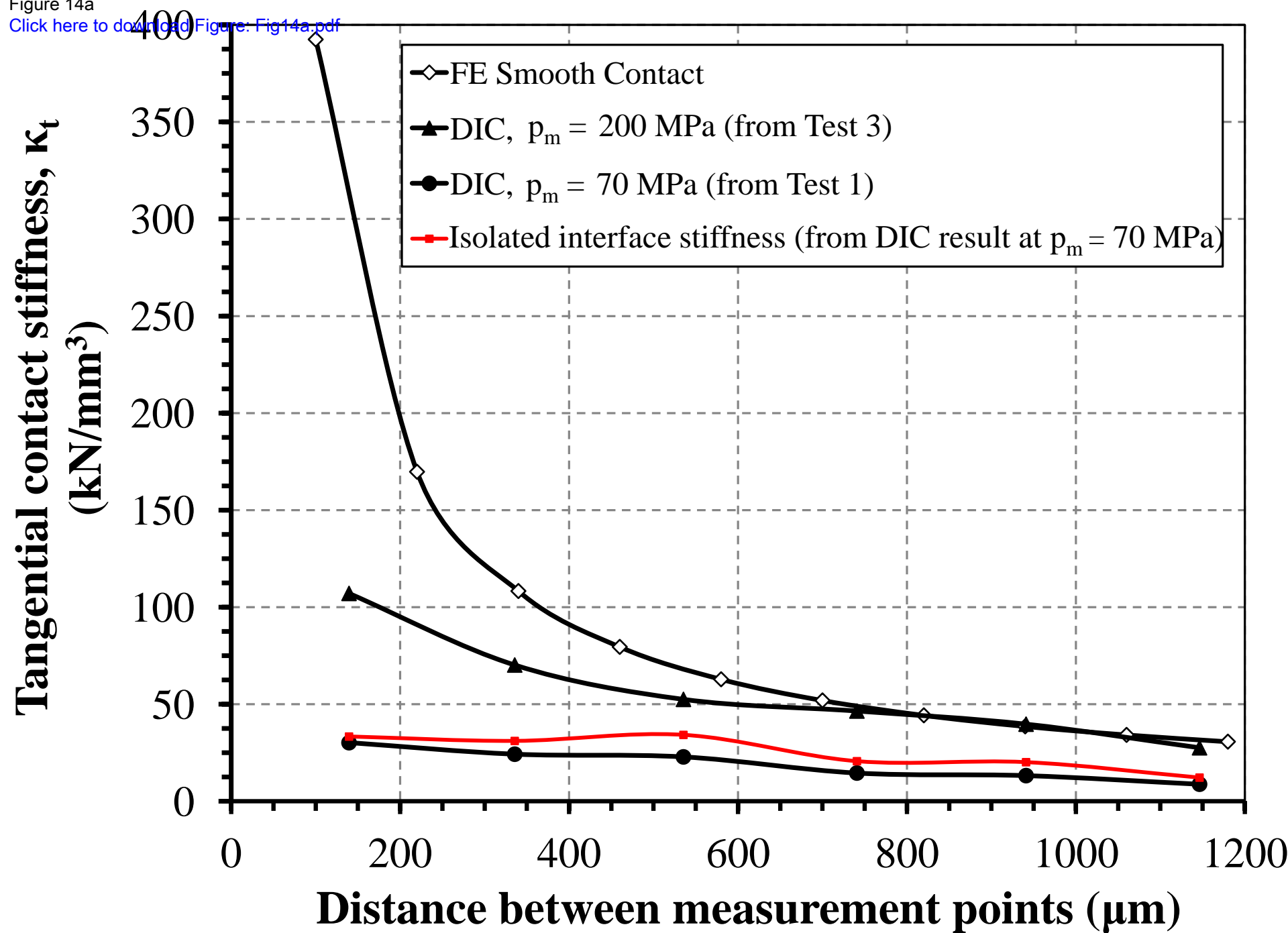


Figure 14b
[Click here to download Figure: Fig14b.pdf](#)

